

Evolution from the Kondo phase to the RKKY phase in the small impurity spacing regime of the two-impurity Anderson model

Hou-Min Du(杜厚旻) and Yu-Liang Liu(刘玉良)†

Citation: Chin. Phys. B, 2025, 34 (**2**): 027102. DOI: 10.1088/1674-1056/ada54f
Journal homepage: http://cpb.iphy.ac.cn; http://iopscience.iop.org/cpb

What follows is a list of articles you may be interested in

Classifying extended, localized and critical states in quasiperiodic lattices via unsupervised learning

Bohan Zheng(郑博涵), Siyu Zhu(朱思宇), Xingping Zhou(周兴平), and Tong Liu(刘通)
Chin. Phys. B, 2025, 34 (**1**): 017103. DOI: 10.1088/1674-1056/ad8cb9

Phase induced localization transition

Tong Liu(刘通), Xingbo Wei(魏兴波), and Youguo Wang(王友国)
Chin. Phys. B, 2024, 33 (**10**): 107103. DOI: 10.1088/1674-1056/ad6a0b

Topological properties of tetratomic Su-Schrieffer-Heeger chains with hierarchical long-range hopping

Guan-Qiang Li(李冠强), Bo-Han Wang(王博涵), Jing-Yu Tang(唐劲羽), Ping Peng(彭娉), and Liang-Wei Dong(董亮伟)
Chin. Phys. B, 2023, 32 (**7**): 077102. DOI: 10.1088/1674-1056/aca7ef

Uniaxial stress effect on quasi-one-dimensional Kondo lattice $CeCo_2Ga_8$

Kangqiao Cheng(程康桥), Binjie Zhou(周斌杰), Cuixiang Wang(王翠香), Shuo Zou(邹烁), Yupeng Pan(潘宇鹏), Xiaobo He(何晓波), Jian Zhang(张健), Fangjun Lu(卢方君), Le Wang(王乐), Youguo Shi(石友国), and Yongkang Luo(罗永康)
Chin. Phys. B, 2022, 31 (**6**): 067104. DOI: 10.1088/1674-1056/ac6339

Ferromagnetism in ZnO with (Mn,Li) codoping

Ma Shi-Jia (马世甲), Lu Peng-Fei (芦鹏飞), Yu Zhong-Yuan (俞重远), Zhao Long (赵龙), Li Qiong-Yao (李琼瑶), Wu Cheng-Jie (武成洁), Ding Lu (丁路)
Chin. Phys. B, 2013, 22 (**3**): 037102. DOI: 10.1088/1674-1056/22/3/037102

RAPID COMMUNICATION

Evolution from the Kondo phase to the RKKY phase in the small impurity spacing regime of the two-impurity Anderson model

Hou-Min Du(杜厚旻) and Yu-Liang Liu(刘玉良)†

Department of Physics, Renmin University of China, Beijing 100872, *China*

(Received 5 November 2024; revised manuscript received 31 December 2024; accepted manuscript online 3 January 2025)

Understanding the quantum critical phenomena is one of the most important and challenging tasks in condensed matter physics and the two-impurity Anderson model (TIAM) is a good starting point for this exploration. To this end, we employ the algebraic equation of motion approach to calculate the TIAM and analytically obtain the explicit single-particle impurity Green function under the soft cut-off approximation (SCA). This approach effectively incorporates the impurity spacing as an intrinsic parameter. By solving the pole equations of the Green function, we have, for the first time, qualitatively calculated the spectral weight functions of the corresponding low-energy excitations. We find that when the impurity spacing is less than one lattice distance, the dynamic Rudermann–Kittel–Kasuya–Yosida (RKKY) interaction effectively enters, resulting in a rapid increase in the spectral weights of the RKKY phase, which ultimately surpass those of the Kondo phase; while the spectral weights of the Kondo phase are strongly suppressed. From the perspective of spectral weights, we further confirm the existence of a crossover from the Kondo phase to the RKKY phase in the TIAM. Based on these results, the reasons for the phenomenon of the Kondo resonance splitting are also discussed.

Keywords: multiple-point correlation function, soft cut-off approximation, Kondo resonance splitting, RKKY interaction

PACS: 71.23.An, 75.30.Hx, 03.65.Fd

DOI: 10.1088/1674-1056/ada54f **CSTR:** 32038.14.CPB.ada54f

1. Introduction

The study of heavy-fermion systems has garnered renewed interest over the past two decades due to the discovery of novel quantum states in the quantum critical region.[1–4] There are two competing energy scales resulting in the above quantum critical phenomena, these are the Kondo temperature and the Rudermann–Kittel–Kasuya–Yosida (RKKY) interaction. Previous studies have shown that there are different types of quantum critical points (QCPs), one is associated with an usual spin-density-wave (SDW) instability by which both sides of the QCP are still the heavy-Fermi-liquid;[5–7] the other with a breakdown of the Kondo effect as well as a vanishing weight of quasiparticles, which leads to a transformation from the heavy-Fermi-liquid to a non-Fermi-liquid as the RKKY interaction increases.[1,8–10] Several mechanisms have been put forward for the latter type, however, no satisfactory theory can give a unified description of the corresponding novel quantum states yet.

Although the nature of the two-impurity Anderson model (TIAM) is somewhat different from the heavy-fermion systems in which there exist phase coherence of each single-ion Kondo singlet[4] and/or long-range magnetic order, it is still a good starting point to study the competition between the Kondo effect and the RKKY interaction.[11] Jones and Varma first implemented a numerical renormalization group (NRG) calculation on a two-impurity Kondo model in which they found a QCP characterized by diverging staggered susceptibility and coefficient of specific heat.[12] However, this QCP is unstable and particle–hole symmetry-protected.[13–20] In fact, the pure TIAM will inevitably generate an effective coupling between impurities which destroys the particle–hole symmetry and leads to a crossover behavior. Interestingly, when appropriate compensating terms at certain impurity spacing are introduced to restore the particle–hole symmetry, the Jones–Varma QCP appears again.[17] Although there has been extensive research on the existence of the QCP, investigations into the TIAM, particularly how the single-ion Kondo singlet phase (Kondo phase) evolves to the intra-impurity singlet phase (RKKY phase) as the impurity spacing continuously varies, are still inadequate.

Experimentally, the two-impurity systems exhibit a remarkable feature in the corresponding critical region, that is in the related differential conductance spectra in absence of external magnetic fields, the Kondo resonance gradually splits into a pseudogap state as the impurity spacing decreases.[21–28] Theoretically, there are primarily two potential sources for the formation of this state: the one is the result of the parity splitting of the even–odd channel of impurities,[29,30] while the other is the spin gap of the singlet–triplet excitation of intra-impurity singlet induced by the RKKY interaction.[31–33] To

†Corresponding author. E-mail: ylliu@ruc.edu.cn

© 2025 Chinese Physical Society and IOP Publishing Ltd. All rights, including for text and data mining, AI training, and similar technologies, are reserved.

specifically determine the source of the Kondo resonance splitting, we need to calculate the corresponding spectral weight functions. Furthermore, through spectral weights, we can directly study the evolution of the above phases with respect to the impurity spacing. However, such calculations are still lacking to date.

In this paper, we analytically calculate the explicit single-particle impurity Green function for the TIAM by using the algebraic equation of motion (AEOM) approach.[34–37] Unlike traditional double-time Green function equations of motion (EOMs) written out in k-space,[38–43] on the contrary, we calculate the AEOMs in lattice space and from which we define the multiple-point correlation functions (see below). There are three salient features in this approach: (a) the correlation effects are completely represented by the multiple-point correlation functions; (b) in terms of the order of the multiple-point correlation functions, the whole set of the AEOMs has a clear hierarchical structure by which we have a transparent cut-off approximation strategy; (c) we use the soft cut-off approximation (SCA) to some high order multiple-point correlation functions, this is essentially different from the usual approximation of the Tyablikov-type[38] in which the high order Green function needs to be factorized into a static correlation function times a low order Green function and then self-consistently solved by using the fluctuation-dissipation theorem. In the limit of infinite impurity spacing, the result will recover to the single-impurity Anderson model.[37] The present scheme can not self-consistently determine the static correlation functions that appear in decoupling processes, however, they do not affect the structure of the Green function and only appear in the spectral weight functions and we treat them as adjustable physical parameters.

The rest of the paper is arranged as follows. In Section 2, we write out the TIAM and give a detailed description of the AEOM approach. In addition, we show a sketch of the hierarchical structure of a set of the AEOMs. We give the analytic expression of the single-particle impurity Green function under $L=1$ order cut-off approximation as well as $L=2$ in Section 3. Based on the Green function under $L=2$ order cut-off approximation, we sequentially study the dynamic RKKY interaction, spectral weight functions and the origination of the Kondo resonance splitting by solving the related pole equations. We close with a conclusion in Section 4. Some of $L=1$ and $L=2$ AEOMs are put in Appendix A. The details of the calculation are put in Appendix B. The explicit expressions of the self-energies of the Kondo and the RKKY are put in Appendix C. The coefficients of the spectral weight functions are put in Appendix D.

2. Model and method

The Hamiltonian of the TIAM on a lattice is as follows:

$$\widehat{H} = \sum_{i,j,\sigma} h_{ij}\widehat{c}^{\dagger}_{i\sigma}\widehat{c}_{j\sigma} + \sum_{\alpha,\sigma}\varepsilon_f \widehat{f}^{\dagger}_{\alpha\sigma}\widehat{f}_{\alpha\sigma} + U\sum_{\alpha}\widehat{n}_{f\alpha\uparrow}\widehat{n}_{f\alpha\downarrow} + V\sum_{\alpha,i,\sigma}\delta_{i\alpha}\left(\widehat{c}^{\dagger}_{i\sigma}\widehat{f}_{\alpha\sigma} + \text{H.c.}\right), \tag{1}$$

where $h_{ij} = -t(\delta_{i,i+1} + \delta_{i+1,i})$ represents the nearest hopping amplitude, the operator $\widehat{c}_{i\sigma}$ ($\widehat{f}_{\alpha\sigma}$) is an usual annihilation operator for conduction electrons (impurities) with spin $\sigma\,(\bar{\sigma}) = \uparrow(\downarrow)$, $\widehat{n}_{f\alpha\uparrow} = \widehat{f}^{\dagger}_{\alpha\uparrow}\widehat{f}_{\alpha\uparrow}$, impurities are indexed by Greek letter $\alpha = \{1,2\}$, ε_f is the energy level of identical spin-1/2 impurities, U is the on-site repulsive Coulomb interaction, V is the hybridization between a conduction electron and an impurity, which is purely local. For the sake of clarity, we interpret the factor $\delta_{i\alpha}$ in the TIAM graphically, as shown in Fig. 1. In this paper, for simplicity, we focus exclusively on the case of local particle–hole symmetry on impurities for a simple cubic lattice at half-filling, where the chemical potential μ equals zero, $2\varepsilon_f + U = 0$, and $\langle\widehat{n}_{f\alpha\sigma}\rangle = 1/2$. Additionally, we concentrate primarily on the regime of local moments and small impurity spacing within the TIAM.

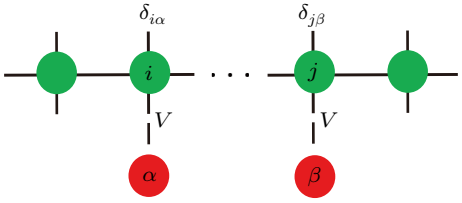


Fig. 1. The configuration of conduction electrons and impurities is shown in one-dimensional direction. The local hybridization V between a conduction electron and an impurity requires a constraint in the Hamiltonian, such as $\delta_{i\alpha}$, to ensure they are located on the same site. The green and red filled circles represent conduction electrons and impurities, respectively.

The single-particle impurity Green function is defined as a 2×2 matrix

$$\mathbb{G} = \begin{pmatrix} G_{\alpha\alpha\sigma} & G_{\alpha\beta\sigma} \\ G_{\beta\alpha\sigma} & G_{\beta\beta\sigma} \end{pmatrix}$$

with

$$G_{\alpha\beta\sigma}(t_1,t_2) = -\mathrm{i}\langle\widehat{T}\widehat{f}_{\alpha\sigma}(t_1)\,\widehat{f}^{\dagger}_{\beta\sigma}(t_2)\rangle, \tag{2}$$

where $\widehat{f}_{\alpha\sigma}$ is defined in the Heisenberg picture, $\langle\cdots\rangle$ represents the average of the ground state of $\widehat{H}$ at zero temperature. Utilizing the Heisenberg EOM of the operator $\widehat{f}_{\alpha\sigma}(t_1)$ and the corresponding equal-time commutator $[\widehat{f}_{\alpha\sigma},\widehat{H}] = \varepsilon_f\widehat{f}_{\alpha\sigma} + V\sum_i\delta_{i\alpha}\widehat{c}_{i\sigma} + U\widehat{n}_{f\alpha\sigma}\widehat{f}_{\alpha\sigma}$, we can obtain the AEOM of above Green function in frequency domain by taking the Fourier transformation $G_{\alpha\beta\sigma}(t_1,t_2) = \int\frac{\mathrm{d}\omega}{2\pi}G_{\alpha\beta\sigma}(\omega)\,\mathrm{e}^{-\mathrm{i}\omega t}$ (set $\hbar = 1$),

$$(\omega-\varepsilon_f)\,G_{\alpha\beta\sigma}(\omega) = \delta_{\alpha\beta} + V\sum_i\delta_{i\alpha}\widetilde{G}_{i\beta\sigma}(\omega)$$

$$+UF^{(n_{f\bar{\sigma}})}_{\alpha\alpha\beta\sigma}(\omega), \tag{3}$$

where $\widetilde{G}_{i\beta\sigma}(t_1,t_2) = -\mathrm{i}\langle\widehat{T}\widehat{c}_{i\sigma}(t_1)\widehat{f}^{\dagger}_{\beta\sigma}(t_2)\rangle$ is the zero order mixed Green function, $F^{(n_{f\bar{\sigma}})}_{\alpha\alpha\beta\sigma}(t_1,t_2) = -\mathrm{i}\langle\widehat{T}\widehat{n}_{f\alpha\bar{\sigma}}(t_1)\widehat{f}_{\alpha\sigma}(t_1)\widehat{f}^{\dagger}_{\beta\sigma}(t_2)\rangle$ is the multiple-point correlation function derived from the repulsive Coulomb interaction term, which includes all of the information about the local and non-local electron correlations.

The AEOMs of the mixed Green function $\widetilde{G}_{i\beta\sigma}(t_1,t_2)$ and the multiple-point correlation function $F^{(n_{f\bar{\sigma}})}_{\alpha\alpha\beta\sigma}(t_1,t_2)$ can be calculated in terms of $[\widehat{c}_{i\bar{\sigma}},\widehat{H}] = h_{ij}\widehat{c}_{j\sigma} + V\sum_{\alpha}\delta_{i\alpha}\widehat{f}_{\alpha\bar{\sigma}}$ and $[\widehat{n}_{f\alpha\bar{\sigma}},\widehat{H}] = V\sum_i \delta_{i\alpha}\widehat{X}^{(-)}_{i\alpha\bar{\sigma}}$,

$$\omega\widetilde{G}_{i\beta\sigma}(\omega) = h_{ij}\widetilde{G}_{j\beta\sigma}(\omega) + V\sum_{\alpha}\delta_{i\alpha}G_{\alpha\beta\sigma}(\omega), \tag{4}$$

$$\begin{aligned}\left(\omega-\varepsilon_f-U\right)F^{(n_{f\bar{\sigma}})}_{\alpha\alpha\beta\sigma}(\omega) &= \delta_{\alpha\beta}\langle\widehat{n}_{f\alpha\bar{\sigma}}\rangle + V\sum_i\delta_{i\alpha}\widetilde{F}^{(n_{f\bar{\sigma}})}_{\alpha i\beta\sigma}(\omega)\\ &\quad + V\sum_i\delta_{i\alpha}F^{(X^{(-)}_{\bar{\sigma}})}_{i\alpha\alpha\beta\sigma}(\omega),\end{aligned} \tag{5}$$

where we have defined the composite operators $\widehat{X}^{(\pm)}_{i\alpha\bar{\sigma}} = \widehat{f}^{\dagger}_{\alpha\bar{\sigma}}\widehat{c}_{i\bar{\sigma}} \pm \widehat{c}^{\dagger}_{i\bar{\sigma}}\widehat{f}_{\alpha\bar{\sigma}}$, and

$$\begin{aligned}F^{(X^{(-)}_{\bar{\sigma}})}_{i\alpha\alpha\beta\sigma}(t_1,t_2) &= -\mathrm{i}\langle\widehat{T}\widehat{X}_{i\alpha\bar{\sigma}}(t_1)\widehat{f}_{\alpha\sigma}(t_1)\widehat{f}^{\dagger}_{\beta\sigma}(t_2)\rangle,\\ \widetilde{F}^{(n_{f\bar{\sigma}})}_{\alpha i\beta\sigma}(t_1,t_2) &= -\mathrm{i}\langle\widehat{T}\widehat{n}_{f\alpha\bar{\sigma}}(t_1)\widehat{c}_{i\bar{\sigma}}(t_1)\widehat{f}^{\dagger}_{\beta\sigma}(t_2)\rangle.\end{aligned}$$

Up to now, if we want to write out more AEOMs of the multiple-point correlation functions, we need calculate more commutation relations. For this reason, we introduce the other four composite operators, $\widehat{Y}^{(\pm)}_{ij\bar{\sigma}} = \widehat{c}^{\dagger}_{j\bar{\sigma}}\widehat{c}_{i\bar{\sigma}} \pm \widehat{c}^{\dagger}_{i\bar{\sigma}}\widehat{c}_{j\bar{\sigma}}$ and $\widehat{Z}^{(\pm)}_{\alpha\beta\bar{\sigma}} = \widehat{f}^{\dagger}_{\beta\bar{\sigma}}\widehat{f}_{\alpha\bar{\sigma}} \pm \widehat{f}^{\dagger}_{\alpha\bar{\sigma}}\widehat{f}_{\beta\bar{\sigma}}$, and then calculate commutation relations between the composite operators and the Hamiltonian $\widehat{H}$, we have

$$\begin{aligned}[\widehat{X}^{(\pm)}_{i\alpha\bar{\sigma}},\widehat{H}] &= h_{ij}\widehat{X}^{(\mp)}_{j\alpha\bar{\sigma}} + \varepsilon_f\widehat{X}^{(\mp)}_{i\alpha\bar{\sigma}} + V\sum_{\beta}\delta_{i\beta}\widehat{Z}^{(\mp)}_{\beta\alpha\bar{\sigma}}\\ &\quad - V\sum_j\delta_{j\alpha}\widehat{Y}^{(\mp)}_{ij\bar{\sigma}} - U\widehat{n}_{f\alpha\bar{\sigma}}\widehat{X}^{(\mp)}_{i\alpha\bar{\sigma}},\end{aligned} \tag{6a}$$

$$\begin{aligned}[\widehat{Y}^{(\pm)}_{ij\bar{\sigma}},\widehat{H}] &= h_{im}\widehat{Y}^{(\mp)}_{mj\bar{\sigma}} - h_{jm}\widehat{Y}^{(\mp)}_{im\bar{\sigma}}\\ &\quad \mp V\sum_{\alpha}\delta_{i\alpha}\widehat{X}^{(\mp)}_{j\alpha\bar{\sigma}} - V\sum_{\alpha}\delta_{j\alpha}\widehat{X}^{(\mp)}_{i\alpha\bar{\sigma}},\end{aligned} \tag{6b}$$

$$\begin{aligned}[\widehat{Z}^{(\pm)}_{\alpha\beta\bar{\sigma}},\widehat{H}] &= V\sum_i\delta_{i\alpha}\widehat{X}^{(\mp)}_{i\beta\bar{\sigma}} \pm V\sum_i\delta_{i\beta}\widehat{X}^{(\mp)}_{i\alpha\bar{\sigma}}\\ &\quad + U\left(\widehat{n}_{f\alpha\sigma} - \widehat{n}_{f\beta\sigma}\right)\widehat{Z}^{(\mp)}_{\alpha\beta\bar{\sigma}}.\end{aligned} \tag{6c}$$

We find that no more new single operator appears except the combinations between old operators, e.g., $n_{f\alpha\bar{\sigma}}X^{(\mp)}_{i\alpha\bar{\sigma}}$. In this sense, all of the commutation relations are closed and we can define all of the multiple-point correlation functions in a compact way,

$$F^{(\{A\})}_{\{\bar{\alpha}\}\alpha\beta\sigma}(t_1,t_2) = -\mathrm{i}\langle\widehat{T}\prod_{k=1}^{L}\widehat{A}^k_{\bar{\alpha}}(t_1)\widehat{f}_{\alpha\sigma}(t_1)\widehat{f}^{\dagger}_{\beta\sigma}(t_2)\rangle, \tag{7a}$$

$$\widetilde{F}^{(\{A\})}_{\{\bar{\alpha}\}i\beta\sigma}(t_1,t_2) = -\mathrm{i}\langle\widehat{T}\prod_{k=1}^{L}\widehat{A}^k_{\bar{\alpha}}(t_1)\widehat{c}_{i\sigma}(t_1)\widehat{f}^{\dagger}_{\beta\sigma}(t_2)\rangle, \tag{7b}$$

where $\widehat{A}_{\bar{\alpha}} = \left\{\widehat{c}_{i\sigma},\widehat{f}_{\alpha\sigma},\widehat{n}_{f\alpha\sigma},\widehat{X}^{(\pm)}_{i\alpha\sigma},\widehat{Y}^{(\pm)}_{ij\sigma},\widehat{Z}^{(\pm)}_{\alpha\beta\sigma}\right\}$, $\bar{\alpha}$ is a set of indices about conduction electrons and impurities, L denotes the number of operators. In this way, the corresponding AEOMs can be readily written out in terms of the above commutation relations. As an example, the AEOMs of $\widetilde{F}^{(n_{f\bar{\sigma}})}_{\alpha i\beta\sigma}(t_1,t_2)$ and $F^{(X^{(\pm)}_{\bar{\sigma}})}_{i\alpha\alpha\beta\sigma}(t_1,t_2)$ can be directly written out by using the commutation relations $[\widehat{c}_{i\bar{\sigma}},\widehat{H}]$, $[\widehat{f}_{\alpha\sigma},\widehat{H}]$, $[\widehat{n}_{f\alpha\bar{\sigma}},\widehat{H}]$ and $[\widehat{X}^{(-)}_{i\alpha\bar{\sigma}},\widehat{H}]$ as well as the definition of the multiple-point correlation functions,

$$\begin{aligned}\omega\widetilde{F}^{(n_{f\bar{\sigma}})}_{\alpha i\beta\sigma}(\omega) &= h_{ij}\widetilde{F}^{(n_{f\bar{\sigma}})}_{\alpha i\beta\sigma}(\omega) + V\sum_{\gamma}\delta_{i\gamma}F^{(n_{f\bar{\sigma}})}_{\alpha\gamma\beta\sigma}(\omega)\\ &\quad + V\sum_i\delta_{j\alpha}\widetilde{F}^{(X^{(-)}_{\bar{\sigma}})}_{j\alpha i\beta\sigma}(\omega),\end{aligned} \tag{8}$$

$$\begin{aligned}&(\omega-\varepsilon_f)F^{(X^{(\pm)}_{\bar{\sigma}})}_{i\alpha\alpha\beta\sigma}(\omega)\\ &= \delta_{\alpha\beta}\langle X^{(\pm)}_{i\alpha\bar{\sigma}}\rangle + h_{ij}F^{(X^{(\mp)}_{\bar{\sigma}})}_{j\alpha\alpha\beta\sigma}(\omega)\\ &\quad -\varepsilon_f F^{(X^{(\mp)}_{\bar{\sigma}})}_{i\alpha\alpha\beta\sigma}(\omega) + V\sum_{\gamma}\delta_{i\gamma}F^{(Z^{(\mp)}_{\bar{\sigma}})}_{\gamma\alpha\alpha\beta\sigma}(\omega)\\ &\quad -V\sum_j\delta_{j\alpha}F^{(Y^{(\mp)}_{\bar{\sigma}})}_{ij\alpha\beta\sigma}(\omega) + V\sum_j\delta_{j\alpha}\widetilde{F}^{(X^{(\pm)}_{\bar{\sigma}})}_{i\alpha j\beta\sigma}(\omega)\\ &\quad +UF^{(X^{(\pm)}_{\bar{\sigma}}n_{f\bar{\sigma}})}_{i\alpha\alpha\alpha\beta\sigma}(\omega),\end{aligned} \tag{9}$$

where the AEOMs of new multiple-point correlation functions are put in Appendix A. Actually, all of correlations enter from $F^{(X^{(\pm)}_{\bar{\sigma}})}_{i\alpha\alpha\beta\sigma}(\omega)$. Continuing the way, we can write out more AEOMs of the higher order multiple-point correlation functions and this set of AEOMs is not closed in the thermodynamic limit, we have to make a cut-off approximation to close the AEOMs. We can use L to denote the order of the multiple-point correlation functions, and then apply the cut-off approximation based on the order. For example, if we make a $L=2$ order cut-off approximation, we need to retain all $L=0$ and $L=1$ order multiple-point correlation functions, as well as the relevant $L=2$ order multiple-point correlation functions that

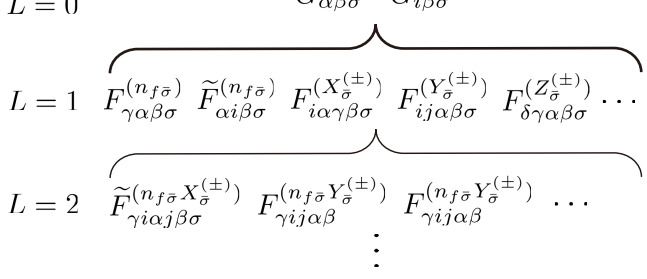


Fig. 2. The hierarchical structure of the whole set of AEOMs is shown. Here, L denotes the number of the composite operators and/or the impurity particle number operators, and represents the order of the multiple-point correlation functions.

make significant contributions, while discarding the other $L=2$ order and higher order multiple-point correlation functions. For clarity, we have outlined a hierarchical structure of this set of AEOMs in Fig. 2.

3. Results

3.1. The $L=1$ order cut-off approximation

As a first step, we will calculate single-particle impurity Green function under $L=1$ order cut-off approximation, where we only retain multiple-point correlation functions $F^{(n_{f\bar{\sigma}})}_{\alpha\alpha\beta\sigma}(\omega)$ and $\widetilde{F}^{(n_{f\bar{\sigma}})}_{\alpha i\beta\sigma}(\omega)$, while discarding the others. Consequently, we have a set of closed AEOMs. The Fourier transformations with respect to conduction electrons and the hopping amplitude are as follows:

$$\widetilde{G}_{i\beta\sigma}(\omega)=\frac{1}{\sqrt{N}}\sum_{\boldsymbol{k}}\widetilde{G}_{\boldsymbol{k}\beta\sigma}(\omega)\,\mathrm{e}^{\mathrm{i}\boldsymbol{k}\cdot\boldsymbol{r}_i},$$
$$h_{ij}=\frac{1}{N}\sum_{\boldsymbol{k}}\varepsilon_{\boldsymbol{k}}\,\mathrm{e}^{\mathrm{i}\boldsymbol{k}\cdot(\boldsymbol{x}_i-\boldsymbol{x}_j)}, \tag{10}$$

where N is the total number of lattice sites and $\varepsilon_{\boldsymbol{k}}$ the dispersion of conduction electrons. By applying the Fourier transformation and utilizing the convolution theorem on Eqs. (3)–(5) and (8), we obtain

$$[\omega-\varepsilon_f-\Gamma_{\alpha\alpha}(\omega)]G_{\alpha\beta\sigma}(\omega)-\Gamma_{\alpha\beta}(\omega)G_{\beta\beta\sigma}(\omega)=\delta_{\alpha\beta}, \tag{11}$$
$$[\omega-\varepsilon_f-U-\Gamma_{\alpha\alpha}(\omega)]F^{(n_{f\bar{\sigma}})}_{\alpha\alpha\beta\sigma}(\omega)$$
$$-\Gamma_{\alpha\beta}(\omega)F^{(n_{f\bar{\sigma}})}_{\alpha\beta\beta\sigma}(\omega)=\delta_{\alpha\beta}\langle\hat{n}_{f\alpha\bar{\sigma}}\rangle, \tag{12}$$

where

$$\Gamma_{\alpha\beta}(\omega+\mathrm{i}0^+)=\frac{V^2}{N}\sum_{\boldsymbol{k}}\frac{\mathrm{e}^{\mathrm{i}\boldsymbol{k}\cdot(\boldsymbol{r}_\alpha-\boldsymbol{r}_\beta)}}{\omega-\varepsilon_{\boldsymbol{k}}+\mathrm{i}0^+} \tag{13}$$

is the hybridization function. The diagonal component $\Gamma_{\alpha\alpha}(\omega)$ typically contributes to the bandwidth of the virtual bound states of impurities, while the non-diagonal component $\Gamma_{\alpha\beta}(\omega)$ arises from the interference between impurities and typically contributes to the effective RKKY interaction. To obtain the single-particle impurity Green function, we need to solve 2×2 and 4×4 matrix equations for Eqs. (11) and (12) respectively; the latter is due to the increased number of the indices. After the algebra, we find

$$G_{\beta\beta\sigma}=\frac{1}{2}\frac{1-\langle\hat{n}_{f\beta\bar{\sigma}}\rangle}{\omega-\Sigma_{L_+}(\omega,r)}+\frac{1}{2}\frac{1-\langle\hat{n}_{f\beta\bar{\sigma}}\rangle}{\omega-\Sigma_{L_-}(\omega,r)}$$
$$+\frac{1}{2}\frac{\langle\hat{n}_{f\beta\bar{\sigma}}\rangle}{\omega-\Sigma_{H_+}(\omega,r)}+\frac{1}{2}\frac{\langle\hat{n}_{f\beta\bar{\sigma}}\rangle}{\omega-\Sigma_{H_-}(\omega,r)}, \tag{14}$$

where $\Sigma_{L_\pm}(\omega,r)=\varepsilon_f+\Gamma_{\alpha\alpha}(\omega)\pm\Gamma_{\alpha\beta}(\omega)$ and $\Sigma_{H_\pm}(\omega,r)=\varepsilon_f+U+\Gamma_{\alpha\alpha}(\omega)\pm\Gamma_{\alpha\beta}(\omega)$ represent the usual lower and higher high-energy Hubbard bands, respectively. Interestingly, each of these bands exhibits a splitting, which indicates magnetic correlation between impurities enters. For the non-diagonal single-particle impurity Green function $G_{\alpha\beta}(\omega)$, the non-diagonal hybridization function $\Gamma_{\alpha\beta}(\omega)$ appears as a prefactor in each term (not shown).

In a tight-binding simple cubic lattice, the dispersion relation is

$$\varepsilon_{\boldsymbol{k}}=-2[\cos(k_x)+\cos(k_y)+\cos(k_z)], \tag{15}$$

where we have set the lattice spacing and hopping amplitude to unity, thus the half bandwidth $D=6$. In this paper, we use the Anderson bandwidth $\Delta=\pi\rho_0V^2$ to determine the hybridization V, where $\rho_0=1/(2D)$ is the constant density of states, and set Δ as an integer multiple of $1/\pi$. By substituting the dispersion relation into Eq. (13), we show the variations of the hybridization function with respect to the impurity spacing in Fig. 3, where $\Gamma_{\alpha\alpha}(\omega)=\Gamma(\omega,0)$ and $\Gamma_{\alpha\beta}(\omega)=\Gamma(\omega,r)$. It is clear that the non-diagonal hybridization function is significantly smaller than the diagonal one in both the real and the imaginary parts. As the impurity spacing goes to infinity, the non-diagonal hybridization function will asymptotically vanish, as will the non-diagonal Green function. In this large impurity spacing limit, the problem reduces to the single-impurity case, and equation (14) will only include the un-split upper and lower Hubbard bands and will be equivalent to the result obtained under the standard Hubbard-I approximation.[40]

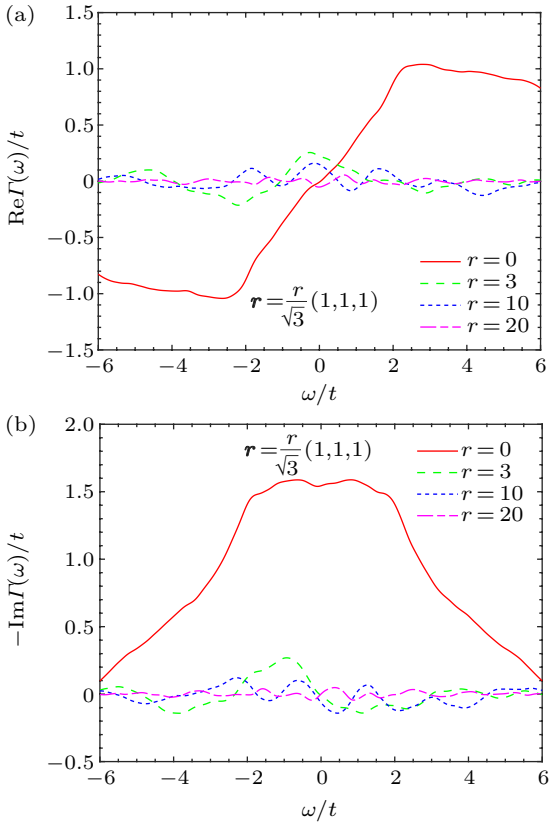


Fig. 3. The hybridization function with different impurity spacings in diagonal direction of the lattice for $\Delta=3/\pi$ and $U=6$.

3.2. The $L=2$ order cut-off approximation

In order to study the competition between the Kondo effect and the RKKY interaction, we need to go beyond $L=1$ order cut-off approximation and examine the higher order AEOMs. To this end, we will next calculate the AEOMs under $L=2$ order cut-off approximation. The most important question for the present problem is how to effectively incorporate both the Kondo effect and the RKKY interaction. For the Kondo effect, we have previously obtained from the high order mixed multiple-point correlation functions $\widetilde{F}^{(Y^{(\pm)}_{\bar{\sigma}})}_{ijl\beta\sigma}(\omega)$.[37] For the RKKY interaction which is mediated by the propagating of particle–hole pairs, we will *a priori* select the multiple-point correlation functions $F^{(Y^{(\pm)}_{\bar{\sigma}})}_{ij\alpha\beta\sigma}(\omega)$ in Eq. (9), which involve $\widetilde{F}^{(Y^{(\pm)}_{\bar{\sigma}})}_{ijl\beta\sigma}(\omega)$, as our starting point. The corresponding AEOMs are as follows:

$$\begin{aligned}
&(\omega-\varepsilon_f)F^{(Y^{(\pm)}_{\bar{\sigma}})}_{ij\alpha\beta\sigma}(\omega)\\
&=\delta_{\alpha\beta}\langle\widehat{Y}^{(\pm)}_{ij\bar{\sigma}}\rangle+h_{im}F^{(Y^{(\mp)}_{\bar{\sigma}})}_{mj\alpha\beta\sigma}(\omega)-h_{jm}F^{(Y^{(\mp)}_{\bar{\sigma}})}_{im\alpha\beta\sigma}(\omega)\\
&\quad\mp V\sum_{\gamma}\delta_{i\gamma}F^{(X^{(\mp)}_{\bar{\sigma}})}_{j\gamma\alpha\beta\sigma}(\omega)-V\sum_{\gamma}\delta_{j\gamma}F^{(X^{(\mp)}_{\bar{\sigma}})}_{i\gamma\alpha\beta\sigma}(\omega)\\
&\quad+V\sum_{l}\delta_{l\alpha}\widetilde{F}^{(Y^{(\pm)}_{\bar{\sigma}})}_{ijl\beta\sigma}(\omega)+UF^{(n_{f\bar{\sigma}}Y^{(\pm)}_{\bar{\alpha}})}_{\alpha ij\alpha\beta\sigma}(\omega),
\end{aligned}\tag{16}$$

where high order AEOMs are

$$\begin{aligned}
&(\omega-\varepsilon_f-U)F^{(n_{f\bar{\sigma}}Y^{(\pm)}_{\bar{\sigma}})}_{\alpha ij\alpha\beta\sigma}(\omega)\\
&=\delta_{\alpha\beta}\langle\widehat{n}_{f\alpha\bar{\sigma}}\widehat{Y}^{(\pm)}_{ij\bar{\sigma}}\rangle+V\sum_{l}\delta_{la}\widetilde{F}^{(n_{f\bar{\sigma}}Y^{(\pm)}_{\bar{\sigma}})}_{\alpha ijl\beta\sigma}(\omega)\\
&\quad\mp V\sum_{\gamma}\delta_{i\gamma}F^{(n_{f\bar{\sigma}}X^{(\mp)}_{\bar{\sigma}})}_{\alpha j\gamma\alpha\beta\sigma}(\omega)-V\sum_{\gamma}\delta_{j\gamma}F^{(n_{f\bar{\sigma}}X^{(\mp)}_{\bar{\sigma}})}_{\alpha i\gamma\alpha\beta\sigma}(\omega)\\
&\quad+h_{im}F^{(n_{f\bar{\sigma}}Y^{(\mp)}_{\bar{\sigma}})}_{\alpha mj\alpha\beta\sigma}(\omega)-h_{jm}F^{(n_{f\bar{\sigma}}Y^{(\mp)}_{\bar{\sigma}})}_{\alpha im\alpha\beta\sigma}(\omega).
\end{aligned}\tag{17}$$

In order to incorporate high order effects while decoupling Eqs. (16) and (17), we apply the SCA to the high order multiple-point correlation functions $F^{(n_{f\bar{\sigma}}X^{(\mp)}_{\bar{\sigma}})}_{\alpha m\gamma\alpha\beta\sigma}(\omega)$ and $\widetilde{F}^{(n_{f\bar{\sigma}}Y^{(\pm)}_{\bar{\sigma}})}_{\alpha ijl\beta\sigma}(\omega)$, where the subscript $m=i,j$. For the former, the summation with respect to γ runs over sites α and β, we restrict γ to be equal to α and neglect the higher order term associated with site β. This leads to the following expression:

$$F^{(n_{f\bar{\sigma}}X^{(\mp)}_{\bar{\sigma}})}_{\alpha m\alpha\alpha\beta\sigma}(\omega)=\frac{1}{2}F^{(X^{(+)}_{\bar{\sigma}})}_{m\alpha\alpha\beta\sigma}(\omega)+\frac{1}{2}F^{(X^{(-)}_{\bar{\sigma}})}_{m\alpha\alpha\beta\sigma}(\omega),\tag{18}$$

which is rigorous. For the latter, we cannot directly apply the SCA to $\widetilde{F}^{(n_{f\bar{\sigma}}Y^{(\pm)}_{\bar{\sigma}})}_{\alpha ijl\beta\sigma}(\omega)$ themselves. Alternatively, we make the SCA to the AEOMs associated with these multiple-point correlation functions and compare them with the low order AEOMs of $\widetilde{F}^{(Y^{(\pm)}_{\bar{\sigma}})}_{ijl\beta\sigma}(\omega)$ (see Appendix B). This leads to the following approximate expressions:

$$\widetilde{F}^{(n_{f\bar{\sigma}}Y^{(\pm)}_{\bar{\sigma}})}_{\alpha ijl\beta\sigma}(\omega)\approx\frac{1}{2}\widetilde{F}^{(Y^{(\pm)}_{\bar{\sigma}})}_{ijl\beta\sigma}(\omega).\tag{19}$$

Using the approximated results obtained above, we substitute Eq. (17) into Eq. (16) to complete the decoupling. It is evident that the decoupling procedure described above has a fundamental difference to the usual mean-field approximation which relies on the mean-field decomposition of high order Green functions. Following the algebra similar to that used in the calculation of Eqs. (11) and (12), we then substitute $F^{(Y^{(\pm)}_{\bar{\sigma}})}_{ij\alpha\beta\sigma}(\omega)$ into $\widetilde{F}^{(Y^{(\pm)}_{\bar{\sigma}})}_{ijl\beta\sigma}(\omega)$, whose AEOM is

$$\begin{aligned}
&(\omega\delta_{lm}-h_{lm})\widetilde{F}^{(Y^{(\pm)}_{\bar{\sigma}})}_{ijm\beta\sigma}(\omega)\\
&=h_{im}\widetilde{F}^{(Y^{(\mp)}_{\bar{\sigma}})}_{mjl\beta\sigma}(\omega)-h_{jm}\widetilde{F}^{(Y^{(\mp)}_{\bar{\sigma}})}_{iml\beta\sigma}(\omega)\\
&\quad\mp V\sum_{\gamma}\delta_{i\gamma}\widetilde{F}^{(X^{(\mp)}_{\bar{\sigma}})}_{j\gamma l\beta\sigma}(\omega)-V\sum_{\gamma}\delta_{j\gamma}\widetilde{F}^{(X^{(\mp)}_{\bar{\sigma}})}_{i\gamma l\beta\sigma}(\omega)\\
&\quad+V\sum_{\alpha}\delta_{l\alpha}F^{(Y^{(\pm)}_{\bar{\sigma}})}_{ij\alpha\beta\sigma}(\omega).
\end{aligned}\tag{20}$$

After completing the above step, we expect to have effectively incorporated the RKKY interaction. Actually, the calculation described above is a self-consistent procedure which effectively incorporates the indirect interaction between impurities through $F^{(Y^{(\pm)}_{\bar{\sigma}})}_{ij\alpha\beta\sigma}(\omega)$. Next, we substitute $\widetilde{F}^{(Y^{(\pm)}_{\bar{\sigma}})}_{ijl\beta\sigma}(\omega)$ into $\widetilde{F}^{(X^{(\pm)}_{\bar{\sigma}})}_{i\alpha j\beta\sigma}(\omega)$, followed by substituting $\widetilde{F}^{(X^{(\pm)}_{\bar{\sigma}})}_{i\alpha jl\beta\sigma}(\omega)$ into $F^{(X^{(\pm)}_{\bar{\sigma}})}_{i\alpha\alpha\beta\sigma}(\omega)$ while neglecting $\mathcal{O}(J^3)$ terms, where $J=4V^2/U$ is the Kondo coupling which naturally arises in the decoupling processes. As a result, we find that, in addition to the self-energies proportional to V^2 that contribute to the Kondo effect, which is the renormalization of energy of the impurity to the Fermi level;[44] there are also additional types of self-energies attributed to the RKKY interaction which are proportional to J^2. Moreover, we find that, similar to the c–f spin-flip static correlation function appears in the spectral weight functions of the Kondo self-energies, which indicates the Kondo phase;[37] the f–f spin-flip static correlation function appears in the spectral weight functions of the RKKY self-energies, which indicates the RKKY phase. The details of the calculation are put in Appendix B.

Our final diagonal single-particle impurity Green function reads

$$\begin{aligned}
&G_{\beta\beta\sigma}(\omega)\\
&=\frac{L_+(\omega,r)}{\omega-\Sigma_{L_+}(\omega,r)}+\frac{L_-(\omega,r)}{\omega-\Sigma_{L_-}(\omega,r)}\\
&\quad+\frac{H_+(\omega,r)}{\omega-\Sigma_{H_+}(\omega,r)}+\frac{H_-(\omega,r)}{\omega-\Sigma_{H_-}(\omega,r)}
\end{aligned}$$

$$+\frac{K_+(\omega,r)}{\omega-\varepsilon_f-\Sigma_{K_+}(\omega,r)}+\frac{K_-(\omega,r)}{\omega-\varepsilon_f-\Sigma_{K_-}(\omega,r)}$$
$$+\frac{R_+(\omega,r)}{\omega+\varepsilon_f-\Sigma_{R_+}(\omega,r)}+\frac{R_-(\omega,r)}{\omega+\varepsilon_f-\Sigma_{R_-}(\omega,r)}, \quad (21)$$

where self-energies $\Sigma_{K_\pm}(\omega)+\varepsilon_f$ and $\Sigma_{R_\pm}(\omega)-\varepsilon_f$ represent the low-energy excitations of the Kondo phase and the RKKY phase, respectively (explicit expressions of the self-energies are put in Appendix C). The corresponding spectral weight functions $K_\pm(\omega,r)$ and $R_\pm(\omega,r)$ take the form of the corresponding frequency dependent factors (see Appendix D) multiplied by $\langle\widehat{S}_\beta^{(+)}\widehat{s}_{\alpha\alpha}^{(-)}\rangle$ and $J_R(\omega,r)\langle\widehat{S}_\beta^{(+)}\widehat{S}_\alpha^{(-)}\rangle$, respectively, where $\widehat{S}_\beta^{(\pm)}=\widehat{f}_{\beta\sigma}^\dagger\widehat{f}_{\beta\bar{\sigma}}$, $\widehat{s}_{ij}^{(\pm)}=\widehat{c}_{i\sigma}^\dagger\widehat{c}_{j\bar{\sigma}}$ and

$$J_R(\omega,r)\approx\frac{J^2}{2N^2}{\sum_{\boldsymbol{k},\boldsymbol{k}'}}'\frac{\mathrm{e}^{\mathrm{i}(\boldsymbol{k}'-\boldsymbol{k})\cdot(\boldsymbol{x}_\alpha-\boldsymbol{x}_\beta)}}{\omega-\varepsilon_f-\varepsilon_{\boldsymbol{k}}+\varepsilon_{\boldsymbol{k}'}}, \quad (22)$$

is the dynamic RKKY interaction that naturally emerges during the decoupling processes, the prime on the sum indicates that $\varepsilon_{\boldsymbol{k}}$ and $\varepsilon_{\boldsymbol{k}'}$ cannot simultaneously appear on the same side of the Fermi surface. Similar to $L=1$ order cut-off approximation, the non-diagonal hybridization function is still linked to each term of the non-diagonal Green function. In addition, in the infinite impurity spacing limit, $G_{\beta\beta\sigma}(\omega)$ will asymptotically recover the result of the single-impurity Kondo problem.[37]

Next, we will primarily focus on the last four terms in Eq. (21) within the regime of small impurity spacing. It is important here to emphasize that the above calculations are grounded in the first principles and represent a dynamic result. To compute the frequency dependent spectral weight functions, we first need to solve the corresponding pole equations.

3.2.1. Solutions of pole equations

In Fig. 4, the poles for $[\omega-\varepsilon_f-\mathrm{Re}\Sigma_{K_+}(\omega+\mathrm{i}0^+,r)]^{-1}$ and $[\omega+\varepsilon_f-\mathrm{Re}\Sigma_{R_+}(\omega+\mathrm{i}0^+,r)]^{-1}$ are shown in the low-energy regime. It is clear that as the impurity spacing decreases from roughly one lattice distance in the diagonal direction $\boldsymbol{r}=(r/\sqrt{3})(1,1,1)$ of the cubic lattice, the poles near $\omega/t\approx0$ gradually split. Additionally, when the impurity spacing is greater than one lattice distance, there is only one solution for the Kondo pole equation, while for the RKKY pole equation, there is no solution. In contrary, there are no solutions for $[\omega-\varepsilon_f-\mathrm{Re}\Sigma_{K_-}(\omega+\mathrm{i}0^+,r)]^{-1}$ and $[\omega+\varepsilon_f-\mathrm{Re}\Sigma_{R_-}(\omega+\mathrm{i}0^+,r)]^{-1}$ in small impurity spacing regime until the spacing roughly approaches one, where only a single solution exists (not shown). The splitting of the two poles is associated with the phenomenon of the Kondo resonance splitting observed in experiments.

It is worth noting that, from the perspective of low-energy excitations, the results presented here appear to contradict previous studies, which suggest that the splitting of the Kondo resonance derives either from the even–odd parity splitting of impurities, where the Kondo effect is still dominant, or from a spin gap induced by an excitation from the intra-impurity singlet to triplet, where the system undergoes a quantum phase transition or a crossover. On the contrary, they both seem to contribute to the splitting here. Essentially, within the Hamiltonian of the pure TIAM, there is no direct interaction between impurities; instead, their interaction must be mediated by the conduction electrons. Although the impurities have a tendency to form a singlet, they cannot be completely decoupled from the Fermi sea, namely, the phase shift of the conduction electrons on the impurities cannot reach $\pi/2$, unless an artificially added compensating term is included to restore the particle–hole symmetry.[17,45] On the other hand, concerning the Kondo singlet, the existence of the Kondo cloud, whose characteristic length scale (single impurity case) is generally larger than the impurity spacing considered in our study, plays a significant role.[46–48] Furthermore, the NRG study on the pure TIAM at certain impurity spacing has indicated that this Kondo resonance splitting phase is the Kondo fixed point where the impurities are under-screened.[17,20] Therefore, we tentatively speculate that the Kondo cloud can be regarded as a background on which the impurities effectively form an intra-impurity singlet. Only having the low-energy excitations, however, is

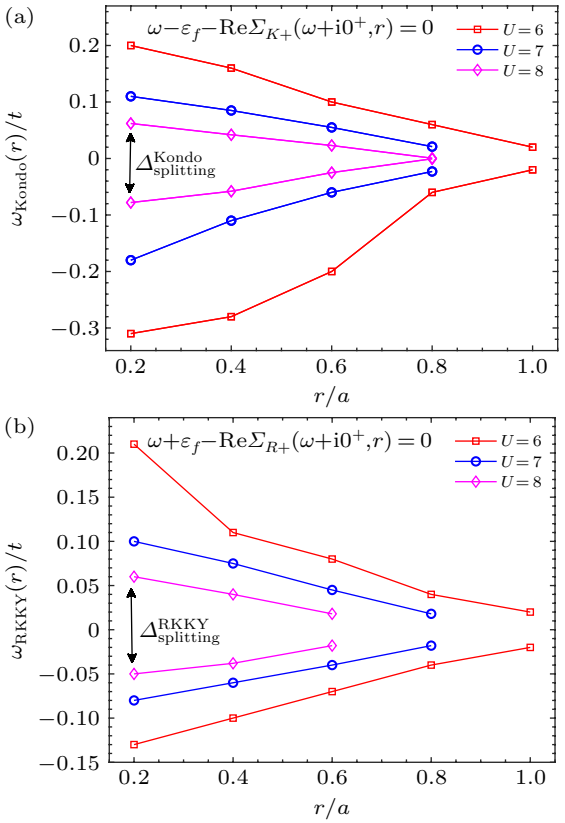


Fig. 4. The poles of $[\omega-\varepsilon_f-\mathrm{Re}\Sigma_{K_+}(\omega+\mathrm{i}0^+,r)]^{-1}$ and $[\omega+\varepsilon_f-\mathrm{Re}\Sigma_{R_+}(\omega+\mathrm{i}0^+,r)]^{-1}$ for different repulsive Coulomb interaction U are shown in the low-energy regime. $\Delta^{\mathrm{Kondo}}_{\mathrm{splitting}}$ and $\Delta^{\mathrm{RKKY}}_{\mathrm{splitting}}$ represent the splitting width of the poles. The parameter used are $\Delta=3/\pi$ and $\boldsymbol{r}=(r/\sqrt{3})(1,1,1)$.

insufficient for the above inference about the Kondo resonance splitting; we still need to consider the corresponding spectral weight functions, even though the static correlation functions cannot be determined from the present scheme.

3.2.2. The dynamic RKKY interaction

Before calculating the spectral weights, we still need to determine the values of the RKKY interaction at different spacings, as the RKKY interaction appears in the corresponding spectral weight functions.

Figure 5(a) shows that the RKKY interactions vary monotonically with the impurity spacing, gradually approaching zero when the spacing exceeds one lattice distance, though some small oscillatory behavior persists thereafter. In fact, this is expected. For rare earth elements, e.g., Ce, although its atomic radius is much larger than one lattice distance (here we assume one lattice distance of about 1 Å), the orbital radius of the deep 4f electrons is less than half a lattice distance.[49] Therefore, within the regime of small impurity spacing we are studying, the RKKY interaction mediated by the conduction electrons effectively enters and competes with the Kondo effect. Additionally, we notice that in this regime, the RKKY interaction is antiferromagnetic and is nearly the same in magnitude for frequencies of different signs.

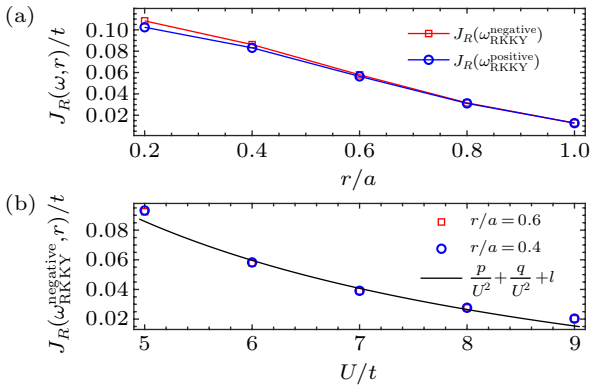


Fig. 5. The dynamic RKKY interaction Eq. (22) for various Coulomb interaction U and impurity spacings as shown. The fitting parameters are $p=0.8231$, $q=-0.0951$ and $l=-0.0749$, and $|p|\gg|q|$ indicates the RKKY interaction is mainly driven by charge fluctuations. The physical parameters used are $U=6$ for upper panel, $\Delta=3/\pi$ and $\boldsymbol{r}=(r/\sqrt{3})(1,1,1)$.

From Fig. 4, we also observe that as the Coulomb interaction U increases, the splitting widths become smaller. To shed some light on this behavior, we plot the RKKY interaction as a function of U at fixed impurity spacing in Fig. 5(b), using the corresponding poles $\omega^{\rm negative}_{\rm RKKY}(r)$ obtained from Fig. 4(b) (without loss of generality, we only select the poles with negative frequencies). We find that the RKKY interaction decreases as U increases. This at least suggests that the splitting of the poles is related to the RKKY interaction to some extent. Additionally, the dependence of the RKKY interaction on U has been studied by fitting. We find that, in the regime of small impurity spacing, the RKKY interaction is nearly proportional to $1/U$ with only minor $1/U^2$ correction, which differs from the conventional $1/U^2$ ($J^2\rho_0$) behavior studied in a spherically symmetric 3D electron gas. This result is consistent with the NRG[17] and the Rayleigh–Schrödinger perturbation theory[50] conducted in simple cubic lattice, which indicate charge fluctuations driven $J_R\propto 1/U$ behavior rather than a Kondo coupling (spin fluctuations) driven $J_R\propto J^2\propto 1/U^2$ in the above regime.

3.2.3. Spectral weight functions

The competition of low-energy excitations of the Kondo and the RKKY phases in a two-impurity Kondo model (TIKM) within the critical region has been studied using the perturbative renormalization group in which non-local vertices are included.[45] However, the TIKM lacks the charge degree of freedom for impurities, while in the small impurity spacing regime of the TIAM, the RKKY interaction is precisely driven mainly by charge fluctuations as we have seen.

The competition between the Kondo and the RKKY phases can be studied directly through the spectral weight functions. To this end, in Fig. 6 we plot the spectral weight functions $K_+(\omega,r)$ and $R_+(\omega,r)$ in Eq. (21) (real part) divided by the c–f static correlation function $\langle\hat{S}^{(+)}_\beta\hat{s}^{(-)}_{\alpha\alpha}\rangle$ and the f–f static correlation function $\langle\hat{S}^{(+)}_\beta\hat{S}^{(-)}_\alpha\rangle$, respectively. This is numerically rigorous. For the former, we find both their values are negative; while for the latter, one is negative and the other is positive. Given that spectral weight functions must be positive definite, we can determine the sign of the related static correlation functions. Thus, we preliminarily draw the following conclusion: in the small spacing regime, (a) the Kondo singlet is preserved and (b) impurities form an intra-impurity singlet along with their excited triplet.

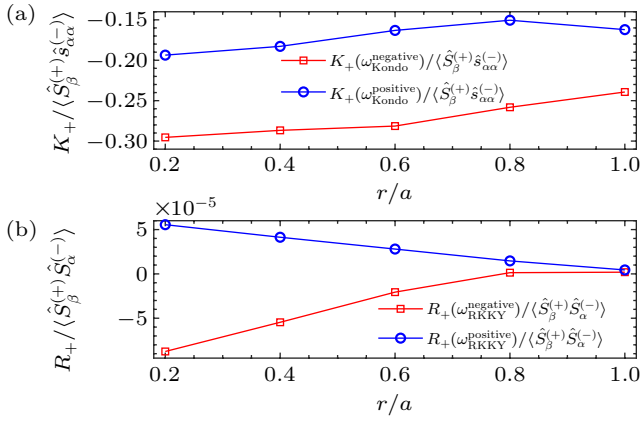


Fig. 6. The spectral weight functions $K_+(\omega,r)$ and $R_+(\omega,r)$ in Eq. (21) divided by $\langle\hat{S}^{(+)}_\beta\hat{s}^{(-)}_{\alpha\alpha}\rangle$ and $\langle\hat{S}^{(+)}_\beta\hat{S}^{(-)}_\alpha\rangle$, respectively. The corresponding poles of each impurity spacing are obtained from Fig. 4, $U=6$ and $\boldsymbol{r}=(r/\sqrt{3})(1,1,1)$.

Now we proceed to qualitatively compare the spectral weight functions of the Kondo and the RKKY phases. There

exists a sum rule related to the c–f static correlation in the Kondo strong coupling limit given by $\int \mathrm{d}^D\boldsymbol{r}\langle\widehat{S}^{(+)}_{\beta}\widehat{s}^{(-)}_{\alpha\alpha}\rangle = -3/4$ in which the integration domain encompasses the range of the Kondo cloud which is much larger than the impurity spacing we study. The envelope function of the integrand has been previously studied in the context of a single impurity case.[17,46–48] For the parameters $\Delta = 3/\pi$ and $U = 6$, there is $\rho_0 J = 0.2026$, we extrapolate the value of the c–f static correlation function in 3D to be roughly $\mathcal{O}(10^{-4})$ from Chapter 4.3 of Ref. [47] in the small spacing regime. Meanwhile, the absolute value of the f–f static correlation function in this regime is expected to be about $\mathcal{O}(1)$.[14,17] As a result, the spectral weight functions of the Kondo and the RKKY phases are of the same order of magnitude. For clarity, we have plotted qualitative comparisons in Fig. 7 and observed points of intersection for frequencies of different signs. For the spectral weights of the RKKY phase, they start from zero at about one lattice distance where the Kondo phase dominates, and gradually increases as the impurity spacing decreases, eventually surpassing the spectral weights of the Kondo phase, indicating that the RKKY phase is becoming increasingly favorable; whereas the spectral weights of the Kondo phase remain almost constant in this regime without significant variation.

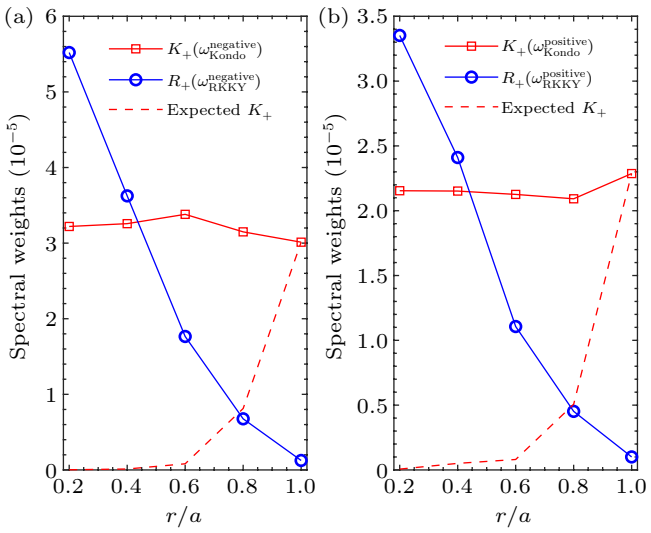


Fig. 7. The qualitative comparisons of the spectral weight functions of the Kondo and the RKKY phases, where the c–f static correlation function $\langle\widehat{S}^{(+)}_{\beta}\widehat{s}^{(-)}_{\alpha\alpha}\rangle$ is extrapolated to be -1×10^{-4} in context of single impurity case from Ref. [47]; and the f–f static correlation function $\langle\widehat{S}^{(+)}_{\beta}\widehat{S}^{(-)}_{\alpha}\rangle$ is set to be ±0.6, plus for the ferromagnetic and minus for the antiferromagnetic. The expected Kondo spectral weights are indicated by the dashed lines. We have used the corresponding poles in Fig. 4. The parameters used are $\Delta = 3/\pi$, $U = 6$ and $\boldsymbol{r} = (r/\sqrt{3})(1,1,1)$.

It should be, however, noted that the calculation of the aforementioned c–f static correlation function was done for the single impurity case, neglecting the influence of the second impurity. It is reasonable to expect that, under the influence of the second impurity, the c–f static correlation function will be suppressed as the impurity spacing decreases. As a result, when the RKKY interaction effectively enters at roughly one lattice distance, we have actually overestimated the spectral weights of the Kondo phase. Meanwhile, with the opening of the pseudogap, we assume that the Kondo correlation turns into an exponential decay at small impurity spacings. We additionally plot the Kondo spectral weight functions with their expected values in Fig. 7 for comparing with the RKKY. In this expected case, the Kondo spectral weight rapidly decreases, indicating that spin fluctuations between conduction electrons and impurities are strongly suppressed. This is also supported by previous study of the RKKY interaction within the small impurity spacing regime, which primarily depends on $1/U$ rather than $1/U^2$ behavior, confirming that the contribution of spin fluctuations in this regime is small. Therefore, the rapid increase of the RKKY spectral weights surpassing the Kondo spectral weight with decreasing impurity distance within the small impurity spacing regime indicates that the system undergoes a crossover, namely, a smooth transition from the Kondo phase to the RKKY phase.

The above discussion provides a qualitative illustration of the crossover phenomenon with respect to the impurity spacing, nevertheless, a more thorough comparison would require a quantitative calculation of the c–f static correlation function in 3D, particularly taking into account the influence of the second impurity. However, computing related static correlation functions remains challenging for methods like perturbative renormalization group[46] and NRG.[17,47] Recently, algebraic approaches, including the two-time Green functions with projective truncation approximation (PTA-EOMGF)[42,48] and algebraic dynamical theory (ADT),[51] have emerged as promising frameworks for addressing these challenges effectively.

For our future work, the related static spin–spin correlation functions could alternatively be determined by artificially adding a spin coupling term with a variational parameter. Using the Hamiltonian with this added term, we compute the single-particle Green function and express the ground-state energy of the original TIAM. Then, we perform a variational calculation on the ground state energy with respect to the variational parameter, thereby obtaining the static correlation functions.

3.2.4. Explanation of the Kondo resonance splitting

In the previous sections, we first solved the pole equations of the Green function, identifying the possible low-energy excitations within the small impurity spacing regime of the TIAM and pointing out their connections to the Kondo resonance splitting, and then studied the spectral weight functions related to these low-energy excitations.

We will now combine the above results to discuss the reason behind the Kondo resonance splitting. The variations of the splitting widths $\Delta^{\text{Kondo}}_{\text{splitting}}$ and $\Delta^{\text{RKKY}}_{\text{splitting}}$ obtained from Fig. 4 with the RKKY interaction are shown in Fig. 8, where each of

them is weighted by the RKKY and the expected Kondo spectral weights from Fig. 7(a) (although there is an asymmetry in the positive and negative frequencies, it does not qualitatively affect the results). The two splitting widths are roughly proportional to the RKKY interaction when it effectively enters, but their slopes are different.

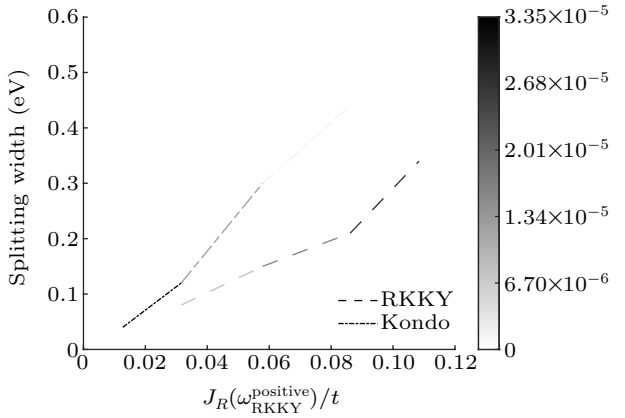


Fig. 8. The dashed and dotted lines represent the splitting widths of the RKKY and the Kondo poles at different values of the dynamic RKKY interaction, respectively weighted by the RKKY and expected Kondo spectral weights from Fig. 7(a). They are roughly proportional to the RKKY interaction. The parameters used are $\Delta = 3/\pi$, $U = 6$ and $\boldsymbol{r} = (r/\sqrt{3})(1,1,1)$.

We first consider the splitting of the RKKY poles, which has a relatively simple origin. It can be viewed as an usual spin gap associated with singlet–triplet excitation of intra-impurity singlet induced by the RKKY interaction. We then turn our attention to the splitting of the Kondo poles, which is more subtle in its mechanism. Generally, the Kondo effect essentially derives from the spin fluctuations that the impurity and the conduction electron spins are in either an up–down or down–up configuration. The Kondo temperature is proportional to the characteristic time scale of the fluctuation. Previous experimental studies on quantum dots have shown that an external magnetic field can split the Kondo resonance into different spin-flip conduction channels.[52] In the present problem, we can inherently view the second impurity as an effective external magnetic field, which is responsible for the splitting of the Kondo poles. As the impurities get closer, the magnetic field felt by one impurity becomes stronger, resulting in a larger effective Zeeman splitting. Interestingly, our results align with those observed in heavy-fermion systems, where the hybridization gap is primarily associated with the coherence temperature.[10]

According to the corresponding spectral weights, when the impurity spacing is less than one lattice distance, the effective Zeeman splitting initially reflects the Kondo resonance splitting. As the dynamic RKKY interaction effectively enters, the system is in a crossover region where the spin gap of the intra-impurity singlet also makes a contribution. When the impurity spacing decreases further, the splitting is primarily contributed by the spin gap.

4. Conclusion

In this work, we have applied the AEOM approach to the TIAM and analytically obtained the single-particle impurity Green function. In this framework, the whole set of AEOMs exhibits a clear hierarchical structure, allowing us to explicitly determine the order of the cut-off approximation. Additionally, we employ the SCA instead of the conventional mean-field decoupling for the high order Green functions, which provides a non-perturbative treatment.

Under $L = 1$ order cut-off approximation, we find that the Green function consists of high-energy part of the splitting upper and lower Hubbard bands due to the non-diagonal hybridization function, and the splitting widths asymptotically vanish as the impurity spacing goes far away.

Under $L = 2$ order cut-off approximation, we incorporate the high order multiple-point correlation functions by using the SCA to them, in which the strong correlation effect effectively enters. We find that in addition to the high energy part, there are additional Kondo and the RKKY self-energies, which are signaled by the c–f $\langle \widehat{S}^{(+)}_{\beta} \widehat{s}^{(-)}_{\alpha\alpha} \rangle$ and the f–f $\langle \widehat{S}^{(+)}_{\beta} \widehat{S}^{(-)}_{\alpha} \rangle$ static correlation functions, respectively.

We have studied the RKKY interaction in a simple cubic lattice and found that for impurity spacing smaller than one lattice distance, it manifests as antiferromagnetic. We then investigate its dependence on the Coulomb interaction U and find that it is proportional to $1/U$, indicating that it is driven by the charge fluctuations rather than by the Kondo coupling in small impurity spacing regime. By estimating the static correlation functions, we qualitatively calculate the spectral weight functions for the Kondo phase and the RKKY phase, discovering that the RKKY spectral weights rapidly increase to surpass the Kondo spectral weight after the RKKY interaction effectively enters. Meanwhile, we argue that the Kondo spectral weight is strongly suppressed due to the influence of the RKKY interaction, leading us to conclude that a crossover occurs in this small impurity spacing regime. Based on these results, we have also discussed the origination of the Kondo resonance splitting. For the RKKY part, the splitting arises from the spin gap of the intra-impurity singlet, while for the Kondo part, it is due to the splitting of spin-flip conduction channels, namely, the effective Zeeman splitting. According to the contributions to the spectral weights in the above regime, the Kondo resonance splitting is initially attributed to the spin-flip conduction channels; then as the dynamic RKKY interaction effectively enters, the system is in a crossover region; when the impurity spacing decreases further, the splitting is primarily contributed by the spin gap.

The present study builds a solid foundation for future study on heavy-fermion systems. Moreover, the generalization of the AEOM approach to calculate other models, particularly the spin systems, is straightforward and effective.

Appendix A: The AEOMs of multiple-point correlation functions

For brevity, all of the AEOMs are written out in frequency domain. For $L=1$ order, we have

$$\begin{aligned}
&(\omega-\varepsilon_f)F^{(Z^{(\pm)}_{\bar\sigma})}_{\gamma\alpha\alpha\beta\sigma}(\omega)\\
=\;&\delta_{\alpha\beta}\langle Z^{(\pm)}_{\gamma\alpha\bar\sigma}\rangle+UF^{(Z^{(\pm)}_{\bar a}n_{f\bar\sigma})}_{\gamma\alpha\alpha\alpha\beta\sigma}(\omega)+V\sum_i\delta_{i\gamma}F^{(X^{(\mp)}_{\bar\sigma})}_{i\alpha\alpha\beta\sigma}(\omega)\\
&-V\sum_i\delta_{i\alpha}F^{(X^{(\mp)}_{\bar\sigma})}_{i\gamma\alpha\beta\sigma}(\omega)+V\sum_i\delta_{i\alpha}\widetilde{F}^{(Z^{(\pm)}_{\bar\sigma})}_{\gamma\alpha i\beta\sigma}(\omega)\\
&+UF^{(n_{f\sigma}Z^{(\mp)}_{\bar\sigma})}_{\gamma\gamma\alpha\alpha\beta\sigma}(\omega),
\end{aligned}\tag{A1}$$

$$\begin{aligned}
&(\omega\delta_{jl}-h_{jl})\widetilde{F}^{(X^{(\pm)}_{\bar\sigma})}_{i\alpha l\beta\sigma}(\omega)\\
=\;&h_{il}\widetilde{F}^{(X^{(\mp)}_{\bar\sigma})}_{l\alpha j\beta\sigma}(\omega)-U\widetilde{F}^{(n_{f\sigma}X^{(\mp)}_{\bar\sigma})}_{\alpha i\alpha j\beta\sigma}(\omega)-V\sum_l\delta_{l\alpha}\widetilde{F}^{(Y^{(\mp)}_{\bar\sigma})}_{il j\beta\sigma}(\omega)\\
&+V\sum_\gamma\delta_{i\gamma}\widetilde{F}^{(Z^{(\pm)}_{\bar\sigma})}_{\gamma\alpha j\beta\sigma}(\omega)-\varepsilon_f\widetilde{F}^{(X^{(\mp)}_{\bar\sigma})}_{i\alpha j\beta\sigma}(\omega)\\
&+V\sum_\gamma\delta_{j\gamma}\widetilde{F}^{(X^{(\pm)}_{\bar\sigma})}_{i\alpha\gamma\beta\sigma}(\omega),
\end{aligned}\tag{A2}$$

$$\begin{aligned}
&(\omega\delta_{ij}-h_{ij})\widetilde{F}^{(Z^{(\pm)}_{\bar\sigma})}_{\gamma\alpha j\beta\sigma}(\omega)\\
=\;&V\sum_\delta\delta_{i\delta}F^{(Z^{(\pm)}_{\bar\sigma})}_{\gamma\alpha\delta\beta\sigma}(\omega)+U\widetilde{F}^{(n_{f\sigma}Z^{(\mp)}_{\bar\sigma})}_{\gamma\gamma\alpha i\beta\sigma}(\omega)\\
&+V\sum_l\delta_{l\alpha}\widetilde{F}^{(X^{(\mp)}_{\bar\sigma})}_{l\gamma i\beta\sigma}(\omega)\pm V\sum_l\delta_{l\alpha}\widetilde{F}^{(X^{(\mp)}_{\bar\sigma})}_{l\gamma i\beta\sigma}(\omega)\\
&-U\widetilde{F}^{(n_{f\sigma}Z^{(\mp)}_{\bar\sigma})}_{\alpha\gamma\alpha i\beta\sigma}(\omega),
\end{aligned}\tag{A3}$$

where dummy variables $\gamma,\delta=\{1,2\}$ are assigned to impurities and l,m to conduction electrons.

For $L=2$ order, we only write out following six AEOMs of the multiple-point correlation functions came from $L=1$ order and simply discard the others:

$$\begin{aligned}
&(\omega\delta_{jl}-h_{jl})\widetilde{F}^{(n_{f\sigma}X^{(\pm)}_{\bar\sigma})}_{\alpha i\alpha l\beta\sigma}(\omega)\\
=\;&\delta_{\alpha\beta}\langle X^{(\pm)}_{i\alpha\bar\sigma}c_{j\sigma}f^\dagger_{\alpha\sigma}\rangle-V\sum_l\delta_{l\alpha}\widetilde{F}^{(n_{f\sigma}Y^{(\mp)}_{\bar\sigma})}_{\alpha il j\beta\sigma}(\omega)\\
&+h_{il}\widetilde{F}^{(n_{f\sigma}X^{(\mp)}_{\bar\sigma})}_{\alpha l\alpha j\beta\sigma}(\omega)-(\varepsilon_f+U)\widetilde{F}^{(n_{f\sigma}X^{(\mp)}_{\bar\sigma})}_{\alpha i\alpha j\beta\sigma}(\omega)\\
&+V\sum_\gamma\delta_{j\gamma}F^{(n_{f\sigma}X^{(\pm)}_{\bar\sigma})}_{\alpha i\alpha\gamma\beta\sigma}(\omega)+V\sum_\gamma\delta_{i\gamma}\widetilde{F}^{(n_{f\sigma}Z^{(\mp)}_{\bar\sigma})}_{\alpha\gamma\alpha j\beta\sigma}(\omega),
\end{aligned}\tag{A4}$$

$$\begin{aligned}
&(\omega\delta_{lm}-h_{lm})\widetilde{F}^{(n_{f\bar\sigma}Y^{(\pm)}_{\sigma})}_{\alpha i jm\beta\sigma}(\omega)\\
=\;&h_{im}\widetilde{F}^{(n_{f\bar\sigma}Y^{(\mp)}_{\sigma})}_{\alpha mjl\beta\sigma}(\omega)-h_{jm}\widetilde{F}^{(n_{f\bar\sigma}Y^{(\pm)}_{\sigma})}_{\alpha iml\beta\sigma}(\omega)\\
&\mp V\sum_\gamma\delta_{i\gamma}\widetilde{F}^{(n_{f\bar\sigma}X^{(\mp)}_{\bar\sigma})}_{\alpha j\gamma l\beta\sigma}(\omega)-V\sum_\gamma\delta_{j\gamma}\widetilde{F}^{(n_{f\bar\sigma}X^{(\mp)}_{\bar\sigma})}_{\alpha i\gamma l\beta\sigma}(\omega)\\
&+V\sum_\gamma\delta_{l\gamma}F^{(n_{f\bar\sigma}Y^{(\pm)}_{\sigma})}_{\alpha ij\gamma\beta\sigma}(\omega),
\end{aligned}\tag{A5}$$

$$\begin{aligned}
&\omega F^{(n_{f\sigma}Z^{(\pm)}_{\bar\sigma})}_{\gamma\gamma\alpha\alpha\beta\sigma}(\omega)\\
=\;&\delta_{\alpha\beta}\langle Z^{(\pm)}_{\gamma\alpha\bar\sigma}f_{\alpha\sigma}f^\dagger_{\gamma\sigma}\rangle+\frac{U}{2}F^{(n_{f\sigma}Z^{(\mp)}_{\bar\sigma})}_{\gamma\gamma\alpha\alpha\beta\sigma}(\omega)\\
&+V\sum_i\delta_{i\gamma}F^{(n_{f\sigma}X^{(\mp)}_{\bar\sigma})}_{\gamma i\alpha\alpha\beta\sigma}(\omega)\pm V\sum_i\delta_{i\alpha}F^{(n_{f\sigma}X^{(\mp)}_{\bar\sigma})}_{\gamma i\gamma\alpha\beta\sigma}(\omega)\\
&+V\sum_i\delta_{i\alpha}\widetilde{F}^{(n_{f\sigma}Z^{(\pm)}_{\bar\sigma})}_{\gamma\gamma\alpha i\beta\sigma}(\omega),
\end{aligned}\tag{A6}$$

where the multiple-point correlation functions with different kinds of composite operators have been neglected, e.g., $F^{(X^{(-)}_{\bar\sigma}Y^{(\pm)}_{\bar\sigma})}_{l\alpha ij\alpha\beta\sigma}(\omega)$.

Appendix B: Details of the calculation

B1. Solutions to the SCA for the AEOMs

We apply the SCA to the AEOMs of $\widetilde{F}^{(n_{f\bar\sigma}Y^{(\pm)}_{\bar\sigma})}_{\alpha ijl\beta\sigma}(\omega)$ rather than themselves. Alternatively, we can make the SCA to $\widetilde{F}^{(n_{f\bar\sigma}X^{(\mp)}_{\bar\sigma})}_{\alpha m\gamma l\beta\sigma}(\omega)$ with $m=i,j$ in Eq. (A5) and similarly restrict the summation that $\gamma=\alpha$. Next, we make an approximation by discarding high order multiple-point correlation functions $F^{(n_{f\bar\sigma}Y^{(\pm)}_{\bar\sigma})}_{\alpha ij\gamma\beta\sigma}(\omega)$, as their contributions have already been incorporated. We also neglect hopping term h_{lm} assumed near the Fermi surface, after which we take the Fourier transformation to Eq. (A5) and obtain

$$\begin{aligned}
&\widetilde{F}^{(n_{f\bar\sigma}Y^{(\pm)}_{\bar\sigma})}_{\alpha\boldsymbol{k}\boldsymbol{k}'l\beta\sigma}(\omega)\\
\approx\;&\frac{V}{2\sqrt{N}}\frac{\omega}{(\omega-\varepsilon_{\boldsymbol{k}}+\varepsilon_{\boldsymbol{k}'})(\omega+\varepsilon_{\boldsymbol{k}}-\varepsilon_{\boldsymbol{k}'})}\\
&\times\left[\mathrm{e}^{-\mathrm{i}\boldsymbol{k}\cdot\boldsymbol{x}_\alpha}\widetilde{F}^{(X^{(+)}_{\bar\sigma})}_{\boldsymbol{k}'\alpha l\beta\sigma}(\omega)-\mathrm{e}^{-\mathrm{i}\boldsymbol{k}'\cdot\boldsymbol{x}_\alpha}\widetilde{F}^{(X^{(+)}_{\bar\sigma})}_{\boldsymbol{k}\alpha l\beta\sigma}(\omega)\right]\\
&-\frac{V}{2\sqrt{N}}\frac{(\varepsilon_{\boldsymbol{k}}-\varepsilon_{\boldsymbol{k}'})}{(\omega-\varepsilon_{\boldsymbol{k}}+\varepsilon_{\boldsymbol{k}'})(\omega+\varepsilon_{\boldsymbol{k}}-\varepsilon_{\boldsymbol{k}'})}\\
&\times\left[\mathrm{e}^{-\mathrm{i}\boldsymbol{k}\cdot\boldsymbol{x}_\alpha}\widetilde{F}^{(X^{(-)}_{\bar\sigma})}_{\boldsymbol{k}'\alpha l\beta\sigma}(\omega)+\mathrm{e}^{-\mathrm{i}\boldsymbol{k}'\cdot\boldsymbol{x}_\alpha}\widetilde{F}^{(X^{(-)}_{\bar\sigma})}_{\boldsymbol{k}\alpha l\beta\sigma}(\omega)\right].
\end{aligned}\tag{B1}$$

By comparing the Fourier transformed AEOMs of $\widetilde{F}^{(Y^{(\pm)}_{\bar\sigma})}_{ijl\beta\sigma}(\omega)$ in Eq. (20) in which we still neglect high order terms $F^{(Y^{(\pm)}_{\bar\sigma})}_{ij\alpha\beta\sigma}(\omega)$ contributing to the RKKY interaction, consequently, we obtain

$$\widetilde{F}^{(n_{f\bar\sigma}Y^{(\pm)}_{\bar\sigma})}_{\alpha ijl\beta\sigma}(\omega)\approx\frac{1}{2}\widetilde{F}^{(Y^{(\pm)}_{\bar\sigma})}_{ijl\beta\sigma}(\omega).$$

Next we substitute the above approximated results into Eq. (17) and take the Fourier transformation, then substitute them into Fourier transformed AEOMs of $F^{(Y^{(\pm)}_{\bar\sigma})}_{ij\alpha\beta\sigma}(\omega)$ to obtain

$$
\begin{aligned}
F^{(Y^{(\pm)}_{\bar\sigma})}_{\boldsymbol{k}\boldsymbol{k}'\alpha\beta\sigma}(\omega) =\ & \frac{V}{4\sqrt{N}}\left(\frac{1}{\omega-\varepsilon_f-\varepsilon_{\boldsymbol{k}}+\varepsilon_{\boldsymbol{k}'}}\mp\frac{2}{\omega-\varepsilon_f+\varepsilon_{\boldsymbol{k}}-\varepsilon_{\boldsymbol{k}'}}+\frac{1}{\omega-\varepsilon_f-U-\varepsilon_{\boldsymbol{k}}+\varepsilon_{\boldsymbol{k}'}}\right)\\
&\times\left[\mathrm{e}^{-\mathrm{i}\boldsymbol{k}\cdot\boldsymbol{x}_\alpha}F^{(X^{(+)}_{\bar\sigma})}_{\boldsymbol{k}'\alpha\alpha\beta\sigma}(\omega)-\mathrm{e}^{-\mathrm{i}\boldsymbol{k}'\cdot\boldsymbol{x}_\alpha}F^{(X^{(+)}_{\bar\sigma})}_{\boldsymbol{k}\alpha\alpha\beta\sigma}(\omega)\right]\\
&-\frac{V}{4\sqrt{N}}\left(\frac{1}{\omega-\varepsilon_f-\varepsilon_{\boldsymbol{k}}+\varepsilon_{\boldsymbol{k}'}}\pm\frac{2}{\omega-\varepsilon_f+\varepsilon_{\boldsymbol{k}}-\varepsilon_{\boldsymbol{k}'}}+\frac{1}{\omega-\varepsilon_f-U-\varepsilon_{\boldsymbol{k}}+\varepsilon_{\boldsymbol{k}'}}\right)\\
&\times\left[\mathrm{e}^{-\mathrm{i}\boldsymbol{k}\cdot\boldsymbol{x}_\alpha}F^{(X^{(-)}_{\bar\sigma})}_{\boldsymbol{k}'\alpha\alpha\beta\sigma}(\omega)+\mathrm{e}^{-\mathrm{i}\boldsymbol{k}'\cdot\boldsymbol{x}_\alpha}F^{(X^{(-)}_{\bar\sigma})}_{\boldsymbol{k}\alpha\alpha\beta\sigma}(\omega)\right]\\
&+\frac{V}{4}\left(\frac{1}{\omega-\varepsilon_f-\varepsilon_{\boldsymbol{k}}+\varepsilon_{\boldsymbol{k}'}}\mp\frac{2}{\omega-\varepsilon_f+\varepsilon_{\boldsymbol{k}}-\varepsilon_{\boldsymbol{k}'}}+\frac{1}{\omega-\varepsilon_f-U-\varepsilon_{\boldsymbol{k}}+\varepsilon_{\boldsymbol{k}'}}\right)\sum_l\delta_{l\alpha}\widetilde{F}^{(Y^{(-)}_{\bar\sigma})}_{\boldsymbol{k}\boldsymbol{k}'l\beta\sigma}(\omega)\\
&+\frac{V}{4}\left(\frac{1}{\omega-\varepsilon_f-\varepsilon_{\boldsymbol{k}}+\varepsilon_{\boldsymbol{k}'}}\pm\frac{2}{\omega-\varepsilon_f+\varepsilon_{\boldsymbol{k}}-\varepsilon_{\boldsymbol{k}'}}+\frac{1}{\omega-\varepsilon_f-U-\varepsilon_{\boldsymbol{k}}+\varepsilon_{\boldsymbol{k}'}}\right)\sum_l\delta_{l\alpha}\widetilde{F}^{(Y^{(+)}_{\bar\sigma})}_{\boldsymbol{k}\boldsymbol{k}'l\beta\sigma}(\omega).
\end{aligned}
\tag{B2}
$$

Then substitute the above AEOMs into Fourier transformed AEOMs of Eq. (20) and after a tedious but straight forward algebra, we obtain

$$
\begin{aligned}
\widetilde{F}^{(Y^{(\pm)}_{\bar\sigma})}_{\boldsymbol{k}\boldsymbol{k}'l\beta\sigma}(\omega) =\ & \frac{V}{\sqrt{N}}\frac{\omega}{(\omega-\varepsilon_{\boldsymbol{k}}+\varepsilon_{\boldsymbol{k}'})(\omega+\varepsilon_{\boldsymbol{k}}-\varepsilon_{\boldsymbol{k}'})}\left[\mathrm{e}^{-\mathrm{i}\boldsymbol{k}\cdot\boldsymbol{x}_\alpha}\widetilde{F}^{(X^{(+)}_{\bar\sigma})}_{\boldsymbol{k}'\alpha l\beta\sigma}(\omega)-\mathrm{e}^{-\mathrm{i}\boldsymbol{k}'\cdot\boldsymbol{x}_\alpha}\widetilde{F}^{(X^{(+)}_{\bar\sigma})}_{\boldsymbol{k}\alpha l\beta\sigma}(\omega)\right]\\
&-\frac{V}{\sqrt{N}}\frac{(\varepsilon_{\boldsymbol{k}}-\varepsilon_{\boldsymbol{k}'})}{(\omega-\varepsilon_{\boldsymbol{k}}+\varepsilon_{\boldsymbol{k}'})(\omega+\varepsilon_{\boldsymbol{k}}-\varepsilon_{\boldsymbol{k}'})}\left[\mathrm{e}^{-\mathrm{i}\boldsymbol{k}\cdot\boldsymbol{x}_\alpha}\widetilde{F}^{(X^{(-)}_{\bar\sigma})}_{\boldsymbol{k}'\alpha l\beta\sigma}(\omega)+\mathrm{e}^{-\mathrm{i}\boldsymbol{k}'\cdot\boldsymbol{x}_\alpha}\widetilde{F}^{(X^{(-)}_{\bar\sigma})}_{\boldsymbol{k}\alpha l\beta\sigma}(\omega)\right]\\
&-\frac{V}{\sqrt{N}}\frac{J}{4U}\left(\frac{1}{\omega-\varepsilon_f-\varepsilon_{\boldsymbol{k}}+\varepsilon_{\boldsymbol{k}'}}\mp\frac{2}{\omega-\varepsilon_f+\varepsilon_{\boldsymbol{k}}-\varepsilon_{\boldsymbol{k}'}}+\frac{1}{\omega-\varepsilon_f-U-\varepsilon_{\boldsymbol{k}}+\varepsilon_{\boldsymbol{k}'}}\right)\\
&\times\left[\mathrm{e}^{-\mathrm{i}\boldsymbol{k}\cdot\boldsymbol{x}_\alpha}\widetilde{F}^{(X^{(+)}_{\bar\sigma})}_{\boldsymbol{k}'\alpha l\beta\sigma}(\omega)-\mathrm{e}^{-\mathrm{i}\boldsymbol{k}'\cdot\boldsymbol{x}_\alpha}\widetilde{F}^{(X^{(+)}_{\bar\sigma})}_{\boldsymbol{k}\alpha l\beta\sigma}(\omega)\right]\\
&-\frac{V}{\sqrt{N}}\frac{J}{4U}\left(\frac{1}{\omega-\varepsilon_f-\varepsilon_{\boldsymbol{k}}+\varepsilon_{\boldsymbol{k}'}}\pm\frac{2}{\omega-\varepsilon_f+\varepsilon_{\boldsymbol{k}}-\varepsilon_{\boldsymbol{k}'}}+\frac{1}{\omega-\varepsilon_f-U-\varepsilon_{\boldsymbol{k}}+\varepsilon_{\boldsymbol{k}'}}\right)\\
&\times\left[\mathrm{e}^{-\mathrm{i}\boldsymbol{k}\cdot\boldsymbol{x}_\alpha}\widetilde{F}^{(X^{(-)}_{\bar\sigma})}_{\boldsymbol{k}'\alpha l\beta\sigma}(\omega)+\mathrm{e}^{-\mathrm{i}\boldsymbol{k}'\cdot\boldsymbol{x}_\alpha}\widetilde{F}^{(X^{(-)}_{\bar\sigma})}_{\boldsymbol{k}\alpha l\beta\sigma}(\omega)\right]-\frac{V}{N}\frac{J}{2U}\sum_\alpha\sum_\gamma\delta_{l\alpha}\frac{\mathrm{e}^{-\mathrm{i}\boldsymbol{k}'\cdot\boldsymbol{x}_\alpha}\mathrm{e}^{-\mathrm{i}\boldsymbol{k}\cdot\boldsymbol{x}_\gamma}}{\omega-\varepsilon_f-\varepsilon_{\boldsymbol{k}}+\varepsilon_{\boldsymbol{k}'}}F^{(Z^{(-)}_{\bar\sigma})}_{\gamma\alpha\alpha\beta\sigma}(\omega),
\end{aligned}
\tag{B3}
$$

where $J=4V^2/U$, $\mathcal{O}(J^2)$ terms have been neglected, and an additional approximation has been made to replace $F^{(X^{(\pm)}_{\bar\sigma})}_{\boldsymbol{k}\alpha\alpha\beta\sigma}(\omega)$ as $F^{(Z^{(-)}_{\bar\sigma})}_{\gamma\alpha\alpha\beta\sigma}(\omega)$,

$$
F^{(X^{(\pm)}_{\bar\sigma})}_{\boldsymbol{k}\alpha\alpha\beta\sigma}(\omega)\approx\frac{V}{\sqrt{N}}\sum_\gamma\frac{\mathrm{e}^{-\mathrm{i}\boldsymbol{k}\cdot\boldsymbol{x}_\gamma}}{\omega-\varepsilon_{\boldsymbol{k}}}F^{(Z^{(\mp)}_{\bar\sigma})}_{\gamma\alpha\alpha\beta\sigma}(\omega),
\tag{B4}
$$

where the multiple-point correlation functions $F^{(Y^{(\pm)}_{\bar\sigma})}_{ij\alpha\beta\sigma}(\omega)$ and $\widetilde{F}^{(X^{(\pm)}_{\bar\sigma})}_{i\alpha j\beta\sigma}(\omega)$ in the Fourier transformed Eq. (9) have been neglected because they have a small correction to the RKKY interaction, and the relation $F^{(Z^{(-)}_{\bar\sigma})}_{\gamma\alpha\alpha\beta\sigma}(\omega)\approx F^{(Z^{(+)}_{\bar\sigma})}_{\gamma\alpha\alpha\beta\sigma}(\omega)$ has been used (see Eq. (B9)). Here we would like to emphasize that the appearance of the RKKY interaction, the last term in Eq. (B3), justify a posteriori the starting point in $L=2$ order calculation.

B2. Solutions to correlation functions of the Kondo and the RKKY

In order to signal and distinguish different poles of the Green function, we need incorporate static correlation functions of the Kondo and the RKKY from Eqs. (A4) and (A6), respectively. For simplicity, under $L=2$ order cut-off approximation, we only retain the corresponding static correlation functions and discard other high order multiple-point correlation functions,

$$
\omega\widetilde{F}^{(n_{f\bar\sigma}X^{(\pm)}_{\bar\sigma})}_{\alpha i\alpha j\beta\sigma}(\omega)\approx-\delta_{\alpha\beta}\langle\widehat{X}^{(\pm)}_{i\alpha\bar\sigma}\widehat{f}^\dagger_{\alpha\sigma}\widehat{c}_{j\sigma}\rangle-\frac{U}{2}\widetilde{F}^{(n_{f\bar\sigma}X^{(\mp)}_{\bar\sigma})}_{\alpha i\alpha j\beta\sigma}(\omega),
\tag{B5}
$$

$$
\omega F^{(n_{f\sigma}Z^{(\pm)}_{\bar\sigma})}_{\gamma\gamma\alpha\alpha\beta\sigma}(\omega)\approx-\delta_{\beta\gamma}\langle\widehat{Z}^{(\pm)}_{\gamma\alpha\bar\sigma}\widehat{f}^\dagger_{\gamma\sigma}\widehat{f}_{\alpha\sigma}\rangle+\frac{U}{2}F^{(n_{f\sigma}Z^{(\mp)}_{\bar\sigma})}_{\gamma\gamma\alpha\alpha\beta\sigma}(\omega).
\tag{B6}
$$

In terms of definitions of composite operators and in the low energy limit $\omega\sim0$, we obtain

$$
\widetilde{F}^{(n_{f\bar\sigma}X^{(\pm)}_{\bar\sigma})}_{\alpha i\alpha j\beta\sigma}(\omega)\approx\mp\frac{2\delta_{\alpha\beta}\langle\widehat{S}^+_\alpha\widehat{s}^{(-)}_{ij}\rangle}{U},
\tag{B7}
$$

$$
F^{(n_{f\sigma}Z^{(\pm)}_{\bar\sigma})}_{\gamma\gamma\alpha\alpha\beta\sigma}(\omega)\approx-\frac{2\delta_{\beta\gamma}\langle\widehat{S}^{(-)}_\alpha\widehat{S}^{(+)}_\gamma\rangle}{U}.
\tag{B8}
$$

Then substitute $F^{(n_{f\sigma}Z^{(\pm)}_{\bar{\sigma}})}_{\gamma\gamma\alpha\alpha\beta\sigma}(\omega)$ into Eq. (A1) and only retain $F^{(Z^{(\pm)}_{\bar{\sigma}})}_{\gamma\alpha\alpha\beta\sigma}(\omega)$, we obtain

$$F^{(Z^{(\pm)}_{\bar{\sigma}})}_{\gamma\alpha\alpha\beta\sigma}(\omega)\approx-\frac{4\delta_{\beta\gamma}\langle\widehat{S}^{(-)}_{\alpha}\widehat{S}^{(+)}_{\gamma}\rangle}{U}, \tag{B9}$$

where due to $\widehat{Z}^{(\pm)}_{\gamma\bar{\sigma}}\widehat{n}_{f\alpha\bar{\sigma}}=\pm\widehat{f}^{\dagger}_{\gamma\bar{\sigma}}\widehat{f}_{\alpha\bar{\sigma}}$, we have used

$$F^{(Z^{(\pm)}_{\bar{\sigma}}n_{f\bar{\sigma}})}_{\gamma\alpha\alpha\beta\sigma}(\omega)=\frac{1}{2}F^{(Z^{(\pm)}_{\bar{\sigma}})}_{\gamma\alpha\beta\sigma}(\omega)-\frac{1}{2}F^{(Z^{(\mp)}_{\bar{\sigma}})}_{\gamma\alpha\beta\sigma}(\omega).$$

B3. Solutions to the multiple-point correlation function $F^{(X^{(\pm)}_{\bar{\sigma}})}_{i\alpha\alpha\beta\sigma}(\omega)$

In order to substitute $\widetilde{F}^{(Y^{(\pm)}_{\bar{\sigma}})}_{ijl\beta\sigma}(\omega)$ into $\widetilde{F}^{(X^{(\pm)}_{\bar{\sigma}})}_{i\alpha j\beta\sigma}(\omega)$, and subsequently substitute $\widetilde{F}^{(X^{(\pm)}_{\bar{\sigma}})}_{i\alpha j\beta\sigma}(\omega)$ into $F^{(X^{(\pm)}_{\bar{\sigma}})}_{i\alpha\alpha\beta\sigma}(\omega)$, we need to take the Fourier transformation of Eq. (B3). However it is impossible to decouple $\widetilde{F}^{(Y^{(\pm)}_{\bar{\sigma}})}_{\boldsymbol{k}\boldsymbol{k}'l\beta\sigma}(\omega)$ and $\widetilde{F}^{(X^{(\pm)}_{\bar{\sigma}})}_{\boldsymbol{p}\alpha l\beta\sigma}(\omega)$ ($\boldsymbol{p}=\boldsymbol{k},\ \boldsymbol{k}'$) during the inverse Fourier transformation because of momentum indices of particle–hole pair $(\omega-\varepsilon_{\boldsymbol{k}}+\varepsilon_{\boldsymbol{k}'})^{-1}$ which couples with $\widetilde{F}^{(X^{(\pm)}_{\bar{\sigma}})}_{\boldsymbol{p}\alpha l\beta\sigma}(\omega)$. To this end, we make an approximation that the energies of the particle $\varepsilon_{\boldsymbol{p}}$ are set to zero and only consider the sum over the holes below the Fermi surface. Later, we arrive at 4×4 matrix problem,

$$\begin{aligned}&\begin{pmatrix}A&B&C&D\\B&A&D&C\\C&D&A&B\\D&C&B&A\end{pmatrix}\begin{pmatrix}\widetilde{F}^{(X^{(-)}_{\bar{\sigma}})}_{i\alpha j\beta\sigma}(\omega)\\\widetilde{F}^{(X^{(+)}_{\bar{\sigma}})}_{i\alpha j\beta\sigma}(\omega)\\\widetilde{F}^{(X^{(-)}_{\bar{\sigma}})}_{i\beta j\beta\sigma}(\omega)\\\widetilde{F}^{(X^{(+)}_{\bar{\sigma}})}_{i\beta j\beta\sigma}(\omega)\end{pmatrix}\\&=\begin{pmatrix}-\frac{J_R(\omega,r)}{U}\langle\widehat{S}^{(-)}_{j}\widehat{S}^{(+)}_{\beta}\rangle\\-\frac{J_R(\omega,r)}{U}\langle\widehat{S}^{(-)}_{j}\widehat{S}^{(+)}_{\beta}\rangle\\-\frac{J_R(\omega,r)}{U}\langle\widehat{S}^{(-)}_{j}\widehat{S}^{(+)}_{\beta}\rangle+2\langle\widehat{S}^{(+)}_{\beta}\widehat{s}^{(-)}_{ij}\rangle\\-\frac{J_R(\omega,r)}{U}\langle\widehat{S}^{(-)}_{j}\widehat{S}^{(+)}_{\beta}\rangle+2\langle\widehat{S}^{(+)}_{\beta}\widehat{s}^{(-)}_{ij}\rangle\end{pmatrix},\end{aligned} \tag{B10}$$

where $A=\omega-\Delta_{\alpha\alpha}(\omega)-2\kappa_{\alpha\alpha}(\omega)-\zeta_{\alpha\alpha}(\omega)$, $B=\varepsilon_f+\eta_{\alpha\alpha}+2\kappa_{\alpha\alpha}(\omega)-\zeta_{\alpha\alpha}(\omega)$, $C=-\Delta_{\alpha\beta}(\omega)-2\kappa_{\alpha\beta}(\omega)-\zeta_{\alpha\beta}(\omega)$ and $D=\eta_{\alpha\beta}(\omega)+2\kappa_{\alpha\beta}(\omega)-\zeta_{\alpha\beta}(\omega)$, and the explicit expressions are put in Appendix C. After solving the above problem, we substitute $\widetilde{F}^{(X^{(\pm)}_{\bar{\sigma}})}_{i\alpha j\beta\sigma}(\omega)$ into $F^{(X^{(\pm)}_{\bar{\sigma}})}_{i\alpha\alpha\beta\sigma}(\omega)$ to obtain

$$\begin{aligned}F^{(X^{(-)}_{\bar{\sigma}})}_{\alpha\alpha\alpha\beta\sigma}(\omega)&=\frac{V\langle\widehat{n}_{f\alpha\bar{\sigma}}\rangle}{D(\omega,r)}\frac{2\Gamma_{\alpha\beta}(\omega)}{\left[\omega-\varepsilon_f-U-\Gamma_{\alpha\alpha}(\omega)-\Gamma_{\alpha\beta}(\omega)\right]\left[\omega-\varepsilon_f-U-\Gamma_{\alpha\alpha}(\omega)+\Gamma_{\alpha\beta}(\omega)\right]}\\&+\frac{V}{D(\omega,r)}\frac{J_R(\omega,r)}{U}\frac{(C+D)\langle\widehat{S}^{(-)}_{\alpha}\widehat{S}^{(+)}_{\beta}\rangle}{(A+B+C+D)(A+B-C-D)},\end{aligned} \tag{B11}$$

$$\begin{aligned}F^{(X^{(-)}_{\bar{\sigma}})}_{\beta\beta\beta\beta\sigma}(\omega)&=\frac{V\langle\widehat{n}_{f\alpha\bar{\sigma}}\rangle}{D(\omega,r)}\frac{2\left[\omega-\varepsilon_f-U-\Gamma_{\alpha\alpha}(\omega)\right]}{\left[\omega-\varepsilon_f-U-\Gamma_{\alpha\alpha}(\omega)-\Gamma_{\alpha\beta}(\omega)\right]\left[\omega-\varepsilon_f-U-\Gamma_{\alpha\alpha}(\omega)+\Gamma_{\alpha\beta}(\omega)\right]}\\&+\frac{V}{D(\omega,r)}\frac{2(A-B)\langle\widehat{S}^{(+)}_{\beta}\widehat{s}^{(-)}_{\alpha\alpha}\rangle}{(A-B+C-D)(A-B-C+D)},\end{aligned} \tag{B12}$$

where the terms associated with $J_R(\omega,0)$ that no spacing enters have been neglected, and $D(\omega,r)$ is put in Appendix D. Finally we substitute above results into Eq. (5) and consequently obtain the single-particle impurity Green function Eq. (20).

Appendix C: Self-energies of the Kondo and the RKKY

The explicit expressions of self-energies are as follows:

$$\begin{aligned}\Sigma_{K_\pm}(\omega,r)&=\eta_{\alpha\alpha}(\omega)\pm\eta_{\alpha\beta}(\omega)+\kappa_{\alpha\alpha}(\omega)\\&\pm\kappa_{\alpha\beta}(\omega)+\Delta_{\alpha\alpha}(\omega)\pm\Delta_{\alpha\beta}(\omega),\end{aligned} \tag{C1}$$

$$\begin{aligned}\Sigma_{R_\pm}(\omega,r)&=-\eta_{\alpha\alpha}(\omega)\mp\eta_{\alpha\beta}(\omega)-\zeta_{\alpha\alpha}(\omega)\\&\pm\zeta_{\alpha\beta}(\omega)+\Delta_{\alpha\alpha}(\omega)\pm\Delta_{\alpha\beta}(\omega),\end{aligned} \tag{C2}$$

where

$$\kappa_{\alpha\beta}(\omega)=\frac{J^2}{4N}\sum_{\boldsymbol{k}}{}'\frac{\mathrm{e}^{\mathrm{i}\boldsymbol{k}\cdot(\boldsymbol{x}_\alpha-\boldsymbol{x}_\beta)}}{\omega-\varepsilon_f-\varepsilon_{\boldsymbol{k}}}, \tag{C3}$$

$$\eta_{\alpha\beta}(\omega)=\frac{V^2}{2N}\sum_{\boldsymbol{k}}{}'\left(\frac{\mathrm{e}^{\mathrm{i}\boldsymbol{k}\cdot(\boldsymbol{x}_\alpha-\boldsymbol{x}_\beta)}}{\omega-\varepsilon_{\boldsymbol{k}}}-\frac{\mathrm{e}^{\mathrm{i}\boldsymbol{k}\cdot(\boldsymbol{x}_\alpha-\boldsymbol{x}_\beta)}}{\omega+\varepsilon_{\boldsymbol{k}}}\right), \tag{C4}$$

$$\Delta_{\alpha\beta}(\omega)=\frac{V^2}{2N}\sum_{\boldsymbol{k}}{}'\left(\frac{\mathrm{e}^{\mathrm{i}\boldsymbol{k}\cdot(\boldsymbol{x}_\alpha-\boldsymbol{x}_\beta)}}{\omega-\varepsilon_{\boldsymbol{k}}}+\frac{\mathrm{e}^{\mathrm{i}\boldsymbol{k}\cdot(\boldsymbol{x}_\alpha-\boldsymbol{x}_\beta)}}{\omega+\varepsilon_{\boldsymbol{k}}}\right), \tag{C5}$$

$$\zeta_{\alpha\beta}(\omega)=\frac{J^2}{8N}\sum_{\boldsymbol{k}}{}'\left(\frac{\mathrm{e}^{\mathrm{i}\boldsymbol{k}\cdot(\boldsymbol{x}_\alpha-\boldsymbol{x}_\beta)}}{\omega-\varepsilon_f-U+\varepsilon_{\boldsymbol{k}}}+\frac{\mathrm{e}^{\mathrm{i}\boldsymbol{k}\cdot(\boldsymbol{x}_\alpha-\boldsymbol{x}_\beta)}}{\omega-\varepsilon_f+\varepsilon_{\boldsymbol{k}}}\right), \tag{C6}$$

and the prime on sum represents that the summation is below the Fermi surface (see Appendix B).

Appendix D: The coefficients in spectral weights

For the sake of clarity, we only show the coefficients of the Kondo and the RKKY components in Eq. (20),

$$K_+(\omega,r)=\left[\frac{1}{k_+(\omega)}+\frac{1}{k_-(\omega)}-\frac{1}{k^U_+(\omega)}-\frac{1}{k^U_-(\omega)}\right]$$

$$\times \frac{V^2}{8D(\omega,r)}\langle \widehat{S}_\beta^{(+)}\widehat{s}_{\alpha\alpha}^{(-)}\rangle, \tag{D1}$$

$$K_-(\omega,r)=\left[\frac{1}{k'_+(\omega)}+\frac{1}{k'_-(\omega)}-\frac{1}{k'^U_+(\omega)}-\frac{1}{k'^U_-(\omega)}\right]$$
$$\times \frac{V^2}{8D(\omega,r)}\langle \widehat{S}_\beta^{(+)}\widehat{s}_{\alpha\alpha}^{(-)}\rangle, \tag{D2}$$

$$R_+(\omega,r)=\left[\frac{1}{r_+(\omega)}-\frac{1}{r_-(\omega)}\right]\frac{J_R(\omega,r)}{64}\langle \widehat{S}_\beta^{(+)}\widehat{S}_\alpha^{(-)}\rangle, \tag{D3}$$

$$R_-(\omega,r)=\left[\frac{1}{r'_+(\omega)}-\frac{1}{r'_-(\omega)}\right]\frac{J_R(\omega,r)}{64}\langle \widehat{S}_\beta^{(+)}\widehat{S}_\alpha^{(-)}\rangle, \tag{D4}$$

where

$$k_\pm(\omega)=\Gamma_{\alpha\alpha}(\omega)\pm\Gamma_{\alpha\beta}(\omega)-\Delta_{\alpha\alpha}(\omega)-\Delta_{\alpha\beta}(\omega)$$
$$-\eta_{\alpha\alpha}(\omega)-\eta_{\alpha\beta}(\omega)-\kappa_{\alpha\alpha}(\omega)-\kappa_{\alpha\beta}(\omega), \tag{D5}$$

$$k'_\pm(\omega)=\Gamma_{\alpha\alpha}(\omega)\pm\Gamma_{\alpha\beta}(\omega)-\Delta_{\alpha\alpha}(\omega)-\Delta_{\alpha\beta}(\omega)$$
$$-\eta_{\alpha\alpha}(\omega)+\eta_{\alpha\beta}(\omega)-\kappa_{\alpha\alpha}(\omega)+\kappa_{\alpha\beta}(\omega), \tag{D6}$$

$$k^U_\pm(\omega)=\Gamma_{\alpha\alpha}(\omega)\pm\Gamma_{\alpha\beta}(\omega)-\Delta_{\alpha\alpha}(\omega)-\Delta_{\alpha\beta}(\omega)$$
$$-\eta_{\alpha\alpha}(\omega)-\eta_{\alpha\beta}(\omega)-\kappa_{\alpha\alpha}(\omega)-\kappa_{\alpha\beta}(\omega)+U, \tag{D7}$$

$$k'^U_\pm(\omega)=\Gamma_{\alpha\alpha}(\omega)\pm\Gamma_{\alpha\beta}(\omega)-\Delta_{\alpha\alpha}(\omega)-\Delta_{\alpha\beta}(\omega)$$
$$-\eta_{\alpha\alpha}(\omega)+\eta_{\alpha\beta}(\omega)-\kappa_{\alpha\alpha}(\omega)+\kappa_{\alpha\beta}(\omega)+U, \tag{D8}$$

$$r_\pm(\omega)=\Gamma_{\alpha\alpha}(\omega)\pm\Gamma_{\alpha\beta}(\omega)-\Delta_{\alpha\alpha}(\omega)-\Delta_{\alpha\beta}(\omega)+2\varepsilon_f$$
$$+\eta_{\alpha\alpha}(\omega)+\eta_{\alpha\beta}(\omega)-\zeta_{\alpha\alpha}(\omega)-\zeta_{\alpha\beta}(\omega), \tag{D9}$$

$$r'_\pm(\omega)=\Gamma_{\alpha\alpha}(\omega)\pm\Gamma_{\alpha\beta}(\omega)-\Delta_{\alpha\alpha}(\omega)-\Delta_{\alpha\beta}(\omega)+2\varepsilon_f$$
$$+\eta_{\alpha\alpha}(\omega)-\eta_{\alpha\beta}(\omega)-\zeta_{\alpha\alpha}(\omega)+\zeta_{\alpha\beta}(\omega), \tag{D10}$$

$$D(\omega,r)=\Omega(\omega,r)-\frac{V^2}{\omega-\varepsilon_f-U-\Gamma_{\alpha\alpha}(\omega)-\Gamma_{\alpha\beta}(\omega)}$$
$$-\frac{V^2}{\omega-\varepsilon_f-U-\Gamma_{\alpha\alpha}(\omega)+\Gamma_{\alpha\beta}(\omega)}, \tag{D11}$$

where

$$\Omega(\omega,r)=\omega-\Phi_{\alpha\alpha}(\omega)+\Phi_{\alpha\beta}(\omega) \tag{D12}$$

with

$$\Phi_{\alpha\beta}(\omega)=\frac{V^2}{2N}\sum_{\boldsymbol{k}}\left(\frac{\mathrm{e}^{\mathrm{i}\boldsymbol{k}\cdot(\boldsymbol{x}_\alpha-\boldsymbol{x}_\beta)}}{\omega-\varepsilon_f-\varepsilon_{\boldsymbol{k}}}+\frac{\mathrm{e}^{\mathrm{i}\boldsymbol{k}\cdot(\boldsymbol{x}_\alpha-\boldsymbol{x}_\beta)}}{\omega-\varepsilon_f+\varepsilon_{\boldsymbol{k}}}\right). \tag{D13}$$

Acknowledgment

Project supported by the National Natural Science Foundation of China (Grant No. 11974420).

References

[1] Coleman P, Pépin C, Si Q and Ramazashvili R 2001 *J. Phys.: Condens. Matter* **13** R723
[2] Löhneysen H V, Rosch A, Vojta M and Wölfle P 2007 *Rev. Mod. Phys.* **79** 1015
[3] Vojta M 2006 *Philosophical Magazine* **86** 1807
[4] Yang Y f, Fisk Z, Lee H O, Thompson J and Pines D 2008 *Nature* **454** 611
[5] Hertz J A 1976 *Phys. Rev. B* **14** 1165
[6] Millis A J 1993 *Phys. Rev. B* **48** 7183
[7] Moriya T 1985 *Spin fluctuations in itinerant electron magnetism* (Berlin: Springer)
[8] Senthil T, Vojta M and Sachdev S 2004 *Phys. Rev. B* **69** 035111
[9] Wölfle P and Abrahams E 2011 *Phys. Rev. B* **84** 041101
[10] Yang Y f 2016 *Reports on Progress in Physics* **79** 074501
[11] Alexander S and Anderson P W 1964 *Phys. Rev.* **133** A1594
[12] Jones B A, Varma C M and Wilkins J W 1988 *Phys. Rev. Lett.* **61** 125
[13] Fye R M and Hirsch J E 1989 *Phys. Rev. B* **40** 4780
[14] He R Q, Dai J and Lu Z Y 2015 *Phys. Rev. B* **91** 155140
[15] Affleck I, Ludwig A W W and Jones B A 1995 *Phys. Rev. B* **52** 9528
[16] Silva J B, Lima W L C, Oliveira W C, Mello J L N, Oliveira L N and Wilkins J W 1996 *Phys. Rev. Lett.* **76** 275
[17] Eickhoff F, Lechtenberg B and Anders F B 2018 *Phys. Rev. B* **98** 115103
[18] Linneweber T, Bünemann J, Mahmoud Z M M and Gebhard F 2017 *J. Phys.: Condens. Matter* **29** 445603
[19] Dong J J, Huang D and Yang Y F 2021 *Phys. Rev. B* **104** L081115
[20] Vojta M, Bulla R and Hofstetter W 2002 *Phys. Rev. B* **65** 140405
[21] Jeong H, Chang A M and Melloch M R 2001 *Science* **293** 2221
[22] Craig N J, Taylor J M, Lester E A, Marcus C M, Hanson M P and Gossard A C 2004 *Science* **304** 565
[23] Bork J, Zhang Y h, Diekhöner L, Borda L, Simon P, Kroha J, Wahl P and Kern K 2011 *Nat. Phys.* **7** 901
[24] Prüser H, Dargel P E, Bouhassoune M, Ulbrich R G, Pruschke T, Lounis S and Wenderoth M 2014 *Nat. Commun.* **5** 5417
[25] Spinelli A, Gerrits M, Toskovic R, Bryant B, Ternes M and Otte A 2015 *Nat. Commun.* **6** 10046
[26] Esat T, Lechtenberg B, Deilmann T, Wagner C, Krüger P, Temirov R, Rohlfing M, Anders F B and Tautz F S 2016 *Nat. Phys.* **12** 867
[27] Chen W, Yan Y, Ren M, Zhang T and Feng D 2022 *Sci. China Phys. Mech. Astron.* **65** 246811
[28] Trishin S, Lotze C, Lohss F, Franceschi G, Glazman L I, von Oppen F and Franke K J 2023 *Phys. Rev. Lett.* **130** 176201
[29] Nishimoto S, Pruschke T and Noack R M 2006 *J. Phys.: Condens. Matter* **18** 981
[30] Jabben T, Grewe N and Schmitt S 2012 *Phys. Rev. B* **85** 045133
[31] Sakai O and Shimizu Y 1992 *J. Phys. Soc. Jpn.* **61** 2333
[32] Zhu L and Zhu J X 2011 *Phys. Rev. B* **83** 195103
[33] Allerdt A, Žitko R and Feiguin A E 2018 *Phys. Rev. B* **97** 045103
[34] Liu Y L 2018 *Int. J. Mod. Phys. B* **32** 1850258
[35] Liu Y L 2019 *Int. J. Mod. Phys. B* **33** 1950355
[36] Liu Y L 2021 *Int. J. Mod. Phys. B* **35** 2150064
[37] Du H M and Liu Y L 2023 *Chin. Phys. B* **32** 047501
[38] Tyablikov S 1959 *Ukrain. Mat.* **11** 287
[39] Zubarev D N 1960 *Soviet Physics Uspekhi* **3** 320
[40] Lacroix C 1981 *J. Phys. F: Metal Phys.* **11** 2389
[41] Chen M L and Wang S J 2007 *Chin. Phys. B* **16** 2096
[42] Fan P, Yang K, Ma K H and Tong N H 2018 *Phys. Rev. B* **97** 165140
[43] Mahmoud Z M M, Bünemann J and Gebhard F 2017 *Physica Status Solidi (b)* **254** 1600842
[44] Haldane F D M 1978 *Phys. Rev. Lett.* **40** 416
[45] Nejati A, Ballmann K and Kroha J 2017 *Phys. Rev. Lett.* **118** 117204
[46] Barzykin V and Affleck I 1998 *Phys. Rev. B* **57** 432
[47] Lechtenberg B 2016 *Equilibrium and nonequilibrium dynamics close to impurity quantum phase transitions* Ph.D. thesis (TU Dortmund)
[48] Fan P, Tong N H and Zhu Z G 2022 *Phys. Rev. B* **106** 155130
[49] Gunnarsson O and Schönhammer K 1987 *High Energy Spectroscopy (Handbook on the Physics and Chemistry of Rare Earths* vol 10) (Elsevier) pp. 103–163
[50] Žitko R and Bonča J 2006 *Phys. Rev. B* **74** 045312
[51] Ding W 2022 arXiv:2202.12082
[52] Heinrich A J, Gupta J A, Lutz C P and Eigler D M 2004 *Science* **306** 466